

Accelerating Dimensionality Reduction in Wave-Resistance Problems through Geometric Operators

Stamatios Stamatatelopoulos^{1,2,*}, Shahroz Khan^{1,3} Panagiotis Kaklis^{1,4}

¹Department of Naval Architecture, Ocean and Marine Engineering, University of Strathclyde, Glasgow (UK)

² Department of Mechanical Engineering, Massachusetts Institute of Technology, Cambridge, (USA)

³BAR Technologies Ltd, Portsmouth (UK)

⁴Foundation for Research & Technology Hellas (FORTH), Institute of Applied & Computational Mathematics (IACM), Division: Numerical Analysis & Computational Science, Group: Data Science, Heraklion, Crete (GR)

Abstract

Reducing the dimensionality and uncertainty of design spaces is a key prerequisite for shape optimisation in computationally intensive fluid problems. However, running these analyses at an offline stage itself poses a computationally demanding task. In this work, we propose a unique framework for the inexpensive implementation of sensitivity analyses for reducing the dimensionality of the design space in wave-resistance problems. At the heart of our approach is the formulation of a geometric operator that leverages, via high-order geometric moments, the underlying connection between geometry and physics, specifically the wave-resistance coefficient (C_w), of ships using the slender body theory based on the well-known Vossers' integral. The resulting geometric operator is computationally inexpensive yet physics-informed and can act as a geometry-based surrogate to drive parametric sensitivities. To analytically demonstrate the capability of the proposed approach, we use a well-known benchmark geometry, namely, the modified Wigley hull. Its simple analytical formulation allows for closed expressions of the geometric operators and exploration of computational domains that would otherwise be inaccessible. In this context, the proposed geometric operator outperforms existing similar approaches by achieving 100% similarity with C_w at a fraction of the computational cost.

Keywords: Dimensionality Reduction; Sensitivity Analysis; Shape Optimisation; Wave Resistance; Geometric Operators

1 Introduction

Identifying satisfactory solutions to physics-based optimisation problems, such as wave resistance minimisation, is a task of fundamental importance in the community of Engineering Design. However, the relevant optimisation algorithms may require evaluating the physics-based objective a number of times, which can be computationally prohibitive. In fact, modern design tools can sometimes prove to be too expensive to run even in cases where a relatively small number of responses need to be evaluated [1]. In tandem with the prohibitive cost of physics-based solvers is the well-known curse of dimensionality [2, 3, 4] which, in the context of sample-based design optimisation, is realised by an explosion in the number of sample evaluations required by optimisation algorithms as the number of optimisation parameters increases. This is precisely the point of intervention of the so-called method of Dimensionality Reduction (DR), whose preliminary objective is to reduce the dimensionality of the design space while keeping the same design variability as the original design space.

In the DR-pertinent literature, there are well-studied unsupervised techniques (e.g., Principal Component Analysis (PCA)[5], auto-encoders [6], etc.) or supervised approaches (e.g., Active Subspace Method (ASM) [7], Sensitivity Analysis (SA) [8]), which may or may not require evaluation of designs' physics, respectively. Among these techniques, PCA, auto-encoders, and ASM extract the latent features of the original design space to create a lower-dimensional subspace while capturing the maximum geometric variability. In contrast, SA is a selection process that identifies parameters that are less sensitive (or insensitive) to physics. As parameters with lower sensitivity have a negligible effect on performance, they can be excluded to reduce the dimensionality of the design space [9, 10, 11].

Compared to SA, unsupervised DR techniques can be computationally efficient since they do not rely on performance labels. However, their effectiveness may be limited when there is no direct correlation with shape modifications. In contrast, SA implementation is more informed because it not only reduces dimensionality but also provides valuable insights into the driving features of designs that contribute to the extreme variability in performance [8, 12]. Consequently, SA enables users to allocate resources more effectively from the early stages of design, thus expediting product development. However, implementing SA can be computationally demanding, especially when an analytical solution is not available, and costly numerical simulations become necessary. Although meta/surrogate models can accelerate SA, constructing the surrogate itself can be a computationally intensive task due to the requirement of evaluating performance labels for dataset creation [13].

*Corresponding author. E-mail address: stamatis@mit.edu (S. Stamatatelopoulos)

Therefore, the aim of this study is to reduce the computational cost of SA for DR purposes by leveraging the underlying connection between physics and geometry. This is achieved by considering that evaluating geometry-based operators is much cheaper compared to their physics-based counterparts. More precisely, for the wave-resistance operator, two geometry-based operators are proposed and tested as surrogate models for SA. It is important to note that the only requirement for the surrogate geometric operators is to be sensitive, in a sense that will be defined below, to the same parameters as the physics-based quantity they are related to. This requirement is much less strenuous when compared to surrogate modelling for optimisation, where the surrogate model must mimic the complete behaviour of the high-fidelity physical model.

To build a vigorous analytical foundation of the proposed approach we used a wigley hull as a test case, which is a standard benchmark geometry in the Naval Architecture domain. It is a simplified mathematical model of ship hulls and is described by simple polynomial representations, making it analytically tractable. The simple analytical expression of the Wigley hull allows for closed forms of geometric operators, thereby reducing computational costs and providing access to computational domains that would otherwise be inaccessible. Leveraging these closed-form solutions at the preliminary design stage, it offers the potential for explicit analysis of the relevant operators, facilitating a deeper understanding of their behaviour and implications.

The remainder of this paper is organised as follows: Section 2 provides a brief overview of the concepts of SA and Uncertainty Analysis (UA) which are fundamental to DR. In Section 3, a general framework is developed for matching physics-based operators to geometry-based ones, two such candidate operators are introduced and the DR framework employed in this study is discussed in more detail. In Section 4, the parametric modeller and the physics-based property, that the methodology developed in the previous section will be applied to, are established. In Section 5 the relevant results are displayed and analysed. Finally in Section 6, conclusive remarks and potential next steps are provided.

2 Background

The design of mathematical models which describe man-made systems reliably is of fundamental importance to the scientific community. The principal role of SA and UA is to answer questions that arise in the design and validation of such models. Such questions can be expressed as (see, e.g., [11, p. 3], [9, p. 183]):

- *How well does the model under consideration represent the underlying physical phenomena?*
- *How far can the calculated results be extrapolated and how can this be achieved?*
- *Which factor or group of factors is most responsible for producing model outputs within or outside specified bounds?*

Specifically, the role of UA given certain model input conditions (such as probability distributions for the input variables) is to *quantify the resulting effect on the output* of the model. On the other hand, the role of SA is to *identify which input variables contributed most to said effect*. Grounded on the above, a reasonable definition of SA and UA can be stated as:

Sensitivity and Uncertainty Analysis is a methodology for the formal evaluation of data and models [11, p. 3]. Uncertainty Analysis is the quantification of uncertainty in the model output given uncertainties in the model input. Sensitivity Analysis is the apportioning of the uncertainty in the model output to different sources of uncertainty in the model input [9, p. 14].

Even though the goals of these two analyses differ, in practice, they are often performed simultaneously and the term *Sensitivity Analysis* has prevailed [10, p. 1]. For the sake of succinctness, this terminology has also been adopted in this paper to refer both to SA and UA.

Having provided a definition of SA that is agreed upon in the literature, we proceed by reviewing the various approaches to perform SA. Out of the many dichotomies of such methods², this brief review will focus on the distinction of *Local* versus *Global* SA since the latter is central to this study. Local SA (LSA) investigates the model behaviour in a small neighbourhood of predetermined points of high interest. On the other hand, Global SA (GSA) investigates the model behaviour over the entire parameter domain.

Historically, LSA is the predecessor of GSA with the first systematic methodology being formulated in [15] as reported in [11, p. 4]. Perhaps the simplest of such methods is the *One at A Time* (OAT), where after a *base point* is chosen, each of the parameters is varied by a specified amount, while all other others are held constant. Comparing the resulting change in model output between parameters can provide insight in their relative importance.

²Other than *Local* vs *Global*, other distinctions include *Statistical* vs *Deterministic* (see [11, p. 8] for a brief discussion) or *Qualitative* vs *Quantitative* (see [14]). In this context, the SA methodology presented in Section 3.4 can be characterised as global, quantitative and deterministic.

Symbolically, given a model $f : \mathbb{R}^n \rightarrow \mathbb{R}$ one assigns a base point $\mathbb{R}^n \ni \mathbf{X}^0 = (x_1^0, \dots, x_n^0)$ and a fixed variation $\epsilon_i \in \mathbb{R}$, $i = 1, \dots, n$ for each parameter. Then, the respective *sensitivity index* for the i^{th} parameter will be $|f(\mathbf{X}_0) - f(x_1^0, \dots, x_i^0 + \epsilon_i, \dots, x_n^0)|$. One of the shortcomings of OAT is that by fixing all parameters other than the i^{th} one, it is impossible to investigate the interactions between two different parameters. For example take $n = 2$: it might be the case that $|f(x_1^0 + \epsilon_1, x_2^0 + \epsilon_2) - f(x_1^0, x_2^0)|$ is much greater than either of the two sensitivity indexes but it will never be evaluated. The more sophisticated *Elementary Effects* method (EE), also known as *Morris* method or *winding stairs* [10], mitigates this issue by performing a number of *steps* where in each step a new OAT experiment is performed [14] and thereafter conclusions for each parameter can be drawn by considering all relevant indices.

The OAT and EE methods belong in the category of *screening* methods, characterised by the subdivision of the domain of each parameter into a number of levels. For a more detailed review of LSA methods, which includes derivative-based methods, the reader is referred to [16]. As stated earlier, in order to investigate the entire parameter domain one employs GSA methods. Such methods include regression-based, variation-based and density-based approaches among others (see [16]). Frameworks for determining which method to employ have been proposed in the literature [14], with the first step being the determination of how close to linear is the relationship of the model output to the model input. More specifically, for any constants $\beta_i \in \mathbb{R}$, the question is how well does the linear relationship $f(\mathbf{X}) = \beta_1 x_1 + \dots + \beta_n x_n$ represent the given model. To handle this issue, one can perform a number of tests such as evaluating the so-called *Pearson correlation coefficient* for each parameter to determine whether its relationship with the output is linear. For any parameters that pass the chosen linearity test satisfactorily, there are readily available measures to evaluate the parameter’s sensitivity such as the Standard Regression Coefficient.

If the user chooses not to make any assumptions about the model or the linearity hypothesis fails by the procedure above, [14] suggest to employ Sobol’s variance-based method. Introduced by Ilya M. Sobol [17], the method is based on the computation of the so called *Sobol’s Index* for each of the input parameters. This method applies to scalar models ($f(\mathbf{X}) \in \mathbb{R}$), however, there do exist generalisations to more than one outputs (see [18]). Since this is the SA approach that has been adopted for this study, more details are provided in Section 3.4.

We proceed to the concept of DR which relates to SA via the last of the questions in the start of this section; *Which factor or group of factors is most influential to the model output?* Having calculated Sobol’s indices $SI_i \in \mathbb{R}$ for all parameter values, a straightforward approach to answering this question is via specifying a threshold value ϵ [19] and filtering the sensitive parameters accordingly. This approach is capable of identifying *subsets* of parameters but fails to determine *linear combinations* of the parameters, which is a feature present in other approaches to DR such as PCA [20] or ASM [7].

Fundamental to the current study is the work of [12]. The authors perform SA on the wave resistance coefficient C_w of a series of ship hulls using the composition of a parametric modeler and a C_w -solver as the model $f(\cdot)$ under investigation. SA is performed globally via the variance-based method of Sobol’s indices as discussed above. Motivated by the well studied correlation between the so-called Sectional Area Curve (SAC)³ of a ship’s hull and ship wave resistance (see [21]) the authors construct a geometry-based operator on ship hulls dubbed *Shape Signature Vector* (SSV) and perform an alternative SA by composing the parametric modeler with the SSV. The two SA approaches are studied for correlation with the expectation that the much cheaper to compute SSV would produce results related to the physics-based solver and thus could be used to expedite the preliminary design stage of hull design. The outcome of this study does show a positive correlation between the two SA’s and this is the starting point for the work relevant to this study.

3 Sensitivity Analysis using Geometric Operators

Let be given a parametric modeller \mathcal{D} of 3D objects embedded in an n -dimensional design space $\mathcal{X} = [a_1, b_1] \times \dots \times [a_n, b_n]$ where each design parameter t_i , $i = 1, \dots, n$ varies continuously in $[a_i, b_i]$. Further, if $\mathcal{P}(\mathcal{D}) \in \mathbb{R}$ is a physics-based property of objects generated by \mathcal{D} , perform SA on \mathcal{D} with \mathcal{P} being the Quantity of Interest (QoI), to identify a subset of $k \leq n$ parameters $I = \{i_1, \dots, i_k\}$ (i.e. $\{t_{i_1}, \dots, t_{i_k}\}$) to which \mathcal{P} is most sensitive to. We aim at identifying a geometry-based operator \mathcal{G} such that performing SA with \mathcal{G} as the QoI, results in a subset of $k' < n$ sensitive parameters $J = \{j_1, \dots, j_{k'}\}$ such that the now reduced-dimensionality design space comprising of the parameters in J can be used for optimisation with \mathcal{P} with acceptable loss of information. This is illustrated in Figure 1,

³SAC represents the longitudinal variation of the cross-sectional area of a ship’s hull below the waterline. The integrated area under the SAC gives the displaced volume and provides an effective and simple description of global geometric properties. At the same time, it is closely related to the resistance and propulsion performance of a ship.

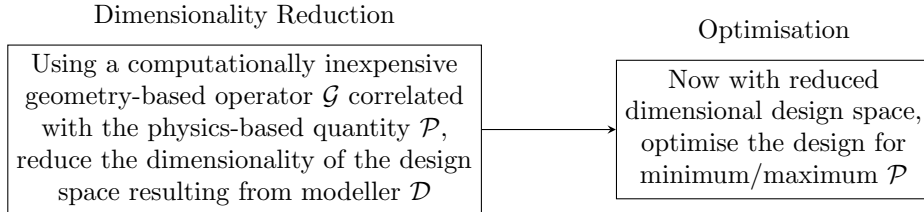


Figure 1: Illustration of the application of the geometric operator \mathcal{G} . It's important to note that \mathcal{G} is not employed in the optimisation step; rather, its use is confined to identifying the most sensitive parameters for dimension reduction. This enables an expedited physics-based optimisation process.

It is important to emphasise that this process produces triplets $(\mathcal{D}, \mathcal{P}, \mathcal{G})$ without any guarantee that the correlation between \mathcal{P} and \mathcal{G} is invariant to \mathcal{D} . It is essential therefore to investigate the dependence of the pair $(\mathcal{P}, \mathcal{G})$ on the parametric modeller \mathcal{D} for, if this dependence is weak, \mathcal{G} can readily be applied to a range of similar parametric modellers. In this effort, the process above can be repeated for constant \mathcal{P} and \mathcal{G} across a set of various parametric modellers $\{\mathcal{D}_1, \mathcal{D}_2, \dots\}$. By verifying the compatibility of an increasing amount of triplets $(\mathcal{D}_i, \mathcal{P}, \mathcal{G})$, the dependence of $(\mathcal{P}, \mathcal{G})$ on the parametric modeller is decreased. For example, in the present case, the aim is to identify a geometric operator \mathcal{G} which is compatible with \mathcal{P} equal to the wave-making resistance coefficient C_w for a set of parametric modelers $\{\mathcal{D}_1, \mathcal{D}_2, \dots\} = \{\mathcal{D}_i : \mathcal{D}_i \text{ produces slender hulls}\}$. The above methodology for identifying triplets $(\{\mathcal{D}_1, \mathcal{D}_2, \dots\}, \mathcal{P}, \mathcal{G})$ is outlined in Figure 2.

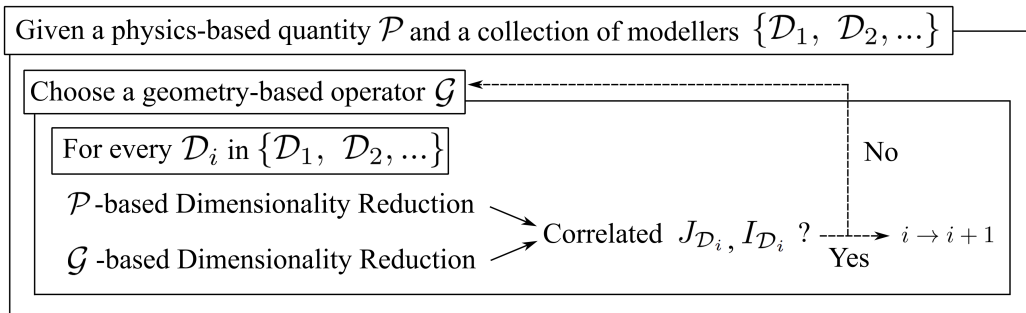


Figure 2: Diagrammatic representation of the methodology for identifying a suitable geometric operator \mathcal{G} compatible with a physics-based quantity \mathcal{P} across a set of parametric modellers $\mathcal{D}_1, \mathcal{D}_2, \dots$.

In this paper, the procedure outlined in Fig. 2 has been applied twice, for two different geometric operators, on a single parametric modeller \mathcal{D}_1 . Both of these geometric operators are based on the concept of geometric moments, introduced in the following three sections. Then, the chosen approach for DR as well as the approach for performing correlation analysis between $J_{\mathcal{D}_i}$ and $I_{\mathcal{D}_i}$ are outlined.

3.1 Geometric Moments

There is a plethora of geometric operators \mathcal{G} which have been studied in the literature, such as the so-called Fourier Descriptors (FD) [22], which extract information from the geometry of the contour, Convexity Measures (CM) ([23]; [24]) or even Elongation Measures [25], which at their simplest form are defined as the width over the length of the bounding box of a 2D shape. In order to apply the procedure in Fig. 2, two desirable attributes on \mathcal{G} are the following:

$$\mathcal{G} \text{ is able to extract enough information from the underlying geometry;} \quad (1a)$$

$$\mathcal{G} \text{ is easy and fast to evaluate for arbitrary geometries.} \quad (1b)$$

In view of the above two points, the two operators \mathcal{G} which have been investigated in this study are based on geometric-moments $M(p, q, r)$. Starting with the definition of $M(p, q, r)$, the s^{th} order moment where $s = p + q + r$ over the solid \mathcal{D} is defined as

$$M(p, q, r) = \iiint_{\mathcal{D}} x^p y^q z^r dx dy dz. \quad (2)$$

From the study of the renowned Problem of Moments [26] it is well known that the geometric moments (2) contain significant information regarding the underlying geometry, which can be used to approximate it and, under certain conditions, even uniquely reconstruct it [27, 28, 29, 30]. For example, the volume of \mathcal{D} is given by $V_{\mathcal{D}} = M(0, 0, 0)$ and its centroid $C = (C_x, C_y, C_z)$ by,

$$C_x = \frac{M(1, 0, 0)}{M(0, 0, 0)}, \quad C_y = \frac{M(0, 1, 0)}{M(0, 0, 0)}, \quad C_z = \frac{M(0, 0, 1)}{M(0, 0, 0)}. \quad (3a)$$

Further, there are numerous procedures for evaluating moments of arbitrary shapes efficiently, one of which is presented in [31] and has been implemented in the scope of this study. It is then evident that geometric-moments easily satisfy (1a) and (1b)

The utility of moments as a mathematical construction has been recognised in various disciplines, with applications starting from probability and statistics [32] and including image analysis [33], signal processing [34], feature extraction [35], computing tomography [36, 37] and inverse potential theory [38, 39] among others. Most importantly, however, they have shown promising results in a context similar to this study [12, 40] via construction of so called Shape Signature Vector (SSV).

3.2 Shape Signature Vector

As mentioned above, significant geometric information carried by \mathcal{D} can be captured with a large enough number of its moments. It is then straightforward to consider as a potential moment-based geometric operator, the vector consisting of all moments up to a certain order. This geometric-based operator is called Shape Signature Vector (SSV) and was first introduced in [12] where it was investigated in an analogous context to the present study. Before introducing the relevant notation, notice that the moments in (2) depend on the position of \mathcal{D} in its ambient space and its scale, two non-desirable characteristics. A translation-invariant form of $M(p, q, r)$ can readily be defined if \mathcal{D} is positioned at its centroid,

$$M_T(p, q, r) = \iiint_{\mathcal{D}} (x - C_x)^p (y - C_y)^q (z - C_z)^r dx dy dz. \quad (4)$$

However, (4) still varies when \mathcal{D} is scaled uniformly by λ , for if we apply the transformation $g(x, y, z) = (\lambda x, \lambda y, \lambda z)$ to (2) over the scaled geometry $\lambda\mathcal{D}$,

$$\begin{aligned} \iiint_{\lambda\mathcal{D}} x^p y^q z^r dx dy dz &= \iiint_{\mathcal{D}} (\lambda x)^p (\lambda y)^q (\lambda z)^r |\det D_g| dx dy dz \\ &= \iiint_{\mathcal{D}} (\lambda x)^p (\lambda y)^q (\lambda z)^r \lambda^3 dx dy dz \\ &= \lambda^{p+q+r+3} M(p, q, r). \end{aligned} \quad (5)$$

Then, looking at (3) and (5) we can write,

$$\begin{aligned} \iiint_{\lambda\mathcal{D}} (x - C_x)^p (y - C_y)^q (z - C_z)^r dx dy dz &= \iiint_{\mathcal{D}} (\lambda x - \lambda C_x)^p (\lambda y - \lambda C_y)^q (\lambda z - \lambda C_z)^r \lambda^3 dx dy dz \\ &= \lambda^{p+q+r+3} M_T(p, q, r). \end{aligned} \quad (6)$$

Since for $\lambda\mathcal{D}$, $M(0, 0, 0) = M_T(0, 0, 0) = V_{\lambda\mathcal{D}} = \lambda^3 V_{\mathcal{D}}$, a scaling invariant moment $M_S(p, q, r)$ and the translation & scaling invariant moment $M_I(p, q, r)$ of \mathcal{D} are given by,

$$M_S(p, q, r) = \frac{M(p, q, r)}{M(0, 0, 0)^{(p+q+r+1)/3}}, \quad (7)$$

$$M_I(p, q, r) = \frac{M_T(p, q, r)}{M_T(0, 0, 0)^{(p+q+r+1)/3}}. \quad (8)$$

Now, given a solid \mathcal{D} , consider the set M_I^s of all scaling and translation invariant moments of \mathcal{D} , $M_I(p, q, r)$ of order s .

$$M_I^s = \{M_I(p, q, r) : p + q + r = s\} \quad (9)$$

For example,

$$M_I^0 = \{M_I(0, 0, 0)\}$$

$$M_I^1 = \{M_I(1, 0, 0), M_I(0, 1, 0), M_I(0, 0, 1)\}$$

$$M_I^2 = \{M_I(2, 0, 0), M_I(1, 1, 0), M_I(1, 0, 1), M_I(0, 2, 0), M_I(0, 1, 1), M_I(0, 0, 2)\}.$$

Notice that all translation invariant moments of order 1 are equal to zero by definition. In light of this, define the Shape Signature Vector (SSV) of order N , as the vector consisting of all elements of M_I^s for $s = 0, 2, \dots, N$,

$$SSV_N = [M_I^0, M_I^2, \dots, M_I^N]. \quad (10)$$

We conclude this section by calculating the cardinality of SSV_N . For each set M_I^s , $\text{Card}(M_I^s) = (s+1)(s+2)/2$ which can be proven inductively. Then since all M_I^s are disjoint,

$$\text{Card}(SSV_N) = \sum_{s=0, s \neq 1}^N \text{Card}(M_I^s) = \sum_{s=0, s \neq 1}^N \frac{(s+1)(s+2)}{2} = \frac{1}{6}N^3 + N^2 + \frac{11}{6}N - 2, \quad N \geq 1. \quad (11)$$

3.3 Slender Body Operator

As will be explained in Section 4, the chosen physics-based quantity in this study is the wave resistance coefficient C_w . The well known correlation between C_w and the SAC of a hull is the starting point for the derivation of the slender body operator. More specifically, in the context of slender body theory, Vossers proposed the following expression for estimating the wave resistance of a slender ship moving at constant velocity U , at water density ρ , with $K = g/U^2$, for g gravitational acceleration [41],

$$\frac{R}{-0.5\rho U^2} = \iint_{\mathbb{R}^2} S''(x)S''(\xi)Y_0(K|x-\xi|)dS'(x)dS'(\xi) \quad (12)$$

where Y_0 is the Bessel function of the second kind, $S(x)$ is the SAC of the ship's hull with $S(x) = 0$ for $x \notin [-L/2, L/2]$ and integration is of Riemann–Stieltjes type. Next, under the assumption that $S'(\pm L/2) = 0$, (12) transforms to the following Riemann integral,

$$\frac{R}{-0.5\rho U^2} = \int_{-L/2}^{L/2} \int_{-L/2}^{L/2} S''(x)S''(\xi)Y_0(K|x-\xi|)dxd\xi, \quad (13)$$

Recall the definition of $Y_0(x)$ to be

$$Y_0(x) = \frac{2}{\pi}(\ln(0.5x) + \gamma)J_0(x) + \frac{2}{\pi} \sum_{k=1}^{\infty} (-1)^{k-1} \frac{(0.25x^2)^k}{(k!)^2} \sum_{j=1}^k \frac{1}{j}, \quad (14)$$

$$J_0(x) = \sum_{k=0}^{\infty} \frac{(-0.25x^2)^k}{(k!)^2}, \quad (15)$$

with J_0 the Bessel function of the first kind. We can then write,

$$\begin{aligned} Y_0(K|x-\xi|) &= \frac{2}{\pi}(\ln(0.5K|x-\xi|) + \gamma)J_0(K|x-\xi|) + \frac{2}{\pi} \sum_{k=1}^{\infty} (-1)^{k-1} \frac{(0.25(K|x-\xi|)^2)^k}{(k!)^2} \sum_{j=1}^k \frac{1}{j} \\ &= \frac{2}{\pi} \ln(|x-\xi|)J_0(K|x-\xi|) + \frac{2}{\pi}(\ln(0.5K) + \gamma)J_0(K|x-\xi|) \\ &\quad + \frac{2}{\pi} \sum_{k=1}^{\infty} (-1)^{k-1} \frac{K^{2k}}{2^{2k}(k!)^2} \left(\sum_{j=1}^k \frac{1}{j} \right) (x-\xi)^{2k} \\ &= \frac{2}{\pi} \ln(|x-\xi|)J_0(K|x-\xi|) + \frac{2}{\pi}(\ln(0.5K) + \gamma) \sum_{k=0}^{\infty} (-1)^k \frac{K^{2k}}{2^{2k}(k!)^2} (x-\xi)^{2k} \\ &\quad + \frac{2}{\pi} \sum_{k=1}^{\infty} (-1)^{k-1} \frac{K^{2k}}{2^{2k}(k!)^2} \left(\sum_{j=1}^k \frac{1}{j} \right) (x-\xi)^{2k} \\ &= \frac{2}{\pi} \ln(|x-\xi|)J_0(K|x-\xi|) + \sum_{k=0}^{\infty} (-1)^k \frac{K^{2k}}{2^{2k-1}(k!)^2\pi} \left(\ln(0.5K) + \gamma - h(k) \right) \end{aligned} \quad (16)$$

where

$$h(k) = \begin{cases} 0, & k = 0 \\ \sum_{j=1}^k \frac{1}{j}, & k > 0. \end{cases} \quad (17)$$

Setting

$$f(k; K) = (-1)^k \frac{K^{2k}}{2^{2k-1}(k!)^2\pi} \left(\ln(0.5K) + \gamma - h(k) \right), \quad (18)$$

we rewrite (14) in its final form

$$Y_0(K|x-\xi|) = \frac{2}{\pi} \ln(|x-\xi|)J_0(K|x-\xi|) + \sum_{k=0}^{\infty} f(K, k). \quad (19)$$

Substituting (19) into (13),

$$\begin{aligned} \int_{-L/2}^{L/2} \int_{-L/2}^{L/2} S''(x)S''(\xi)Y_0(K|x-\xi|)dxd\xi &= \frac{2}{\pi} \int_{-L/2}^{L/2} \int_{-L/2}^{L/2} S''(x)S''(\xi) \ln(|x-\xi|)J_0(K|x-\xi|)dxd\xi \\ &\quad + \sum_{k=0}^{\infty} f(k; K)I_k \end{aligned} \quad (20)$$

with

$$I_k = \int_{-L/2}^{L/2} \int_{-L/2}^{L/2} S''(x)S''(\xi)(x-\xi)^{2k} dx d\xi. \quad (21)$$

We will now show I_k can be expressed as a quadratic polynomial in moments of the type $M(n, 0, 0)$, in view of which we introduce the following notation,

$$M_n \equiv M(n, 0, 0). \quad (22)$$

To proceed, expand $(x - \xi)^{2k}$,

$$\begin{aligned} I_k &= \int_{-L/2}^{L/2} \int_{-L/2}^{L/2} S''(x)S''(\xi) \sum_{i=0}^{2k} \binom{2k}{i} (-1)^i x^{2k-i} \xi^i dx d\xi \\ &= \sum_{i=0}^{2k} \binom{2k}{i} (-1)^i \left(\int_{-L/2}^{L/2} S''(x)x^{2k-i} dx \right) \left(\int_{-L/2}^{L/2} S''(\xi)\xi^i d\xi \right). \end{aligned} \quad (23)$$

It is evident that we must investigate the integral

$$II_N = \int_{-L/2}^{L/2} S''(x)x^N dx. \quad (24)$$

Integrating twice by parts,

$$\begin{aligned} II_N &= \left[S'(x)x^N \right]_{-L/2}^{L/2} - N \int_{-L/2}^{L/2} S'(x)x^{N-1} dx \\ &= \left[S'(x)x^N \right]_{-L/2}^{L/2} - N \left[S(x)x^{N-1} \right]_{-L/2}^{L/2} + N(N-1) \int_{-L/2}^{L/2} S(x)x^{N-2} dx \\ &= \left[S'(x)x^N \right]_{-L/2}^{L/2} - N \left[S(x)x^{N-1} \right]_{-L/2}^{L/2} + N(N-1)M_{N-2}, \quad N \geq 2. \end{aligned} \quad (25)$$

Setting $M_{-1} \equiv M_{-2} = 0$ we extend (25) to all $N \geq 0$ without any effect on the ensuing calculations, which allows for less cumbersome notation in what follows. Now, looking at (23) it is evident that we must expand $II_{2k-i}II_i$,

$$\begin{aligned} II_{2k-i}II_i &= \left(\left[S'(x)x^{2k-i} \right]_{-L/2}^{L/2} - (2k-i) \left[S(x)x^{2k-i-1} \right]_{-L/2}^{L/2} + (2k-i)(2k-i-1)M_{2k-i-2} \right) \\ &\quad \cdot \left(\left[S'(x)x^i \right]_{-L/2}^{L/2} - i \left[S(x)x^{i-1} \right]_{-L/2}^{L/2} + i(i-1)M_{i-2} \right) \\ &= \left(\left[S'(x)x^{2k-i} \right]_{-L/2}^{L/2} - (2k-i) \left[S(x)x^{2k-i-1} \right]_{-L/2}^{L/2} \right) \left(\left[S'(x)x^i \right]_{-L/2}^{L/2} - i \left[S(x)x^{i-1} \right]_{-L/2}^{L/2} \right) \\ &\quad + (2k-i)(2k-i-1) \left(\left[S'(x)x^i \right]_{-L/2}^{L/2} - i \left[S(x)x^{i-1} \right]_{-L/2}^{L/2} \right) M_{2k-i-2} \\ &\quad + i(i-1) \left(\left[S'(x)x^{2k-i} \right]_{-L/2}^{L/2} - (2k-i) \left[S(x)x^{2k-i-1} \right]_{-L/2}^{L/2} \right) M_{i-2} \\ &\quad + i(i-1)(2k-i)(2k-i-1)M_{i-2}M_{2k-i-2}. \end{aligned} \quad (26)$$

Before substituting (26) into (23), notice that a significant number of terms is repeated across the summation. For example, the last term in (26) at i will be identical to that at $2k-i$. Same terms can easily be grouped together by noticing that for any $g(N)$

$$\sum_{i=0}^{2k} \binom{2k}{i} (-1)^i g(i)g(2k-i) = \left(\sum_{i=k}^k + 2 \sum_{i=0}^{k-1} \right) \binom{2k}{i} (-1)^i g(i)g(2k-i). \quad (27)$$

Then looking at (26) and (27), set

$$c^k = \left(\sum_{i=k}^k + 2 \sum_{i=0}^{k-1} \right) \binom{2k}{i} (-1)^i \left(\left[S'(x)x^{2k-i} \right]_{-L/2}^{L/2} - (2k-i) \left[S(x)x^{2k-i-1} \right]_{-L/2}^{L/2} \right) \cdot \left(\left[S'(x)x^i \right]_{-L/2}^{L/2} - i \left[S(x)x^{i-1} \right]_{-L/2}^{L/2} \right), \quad (28a)$$

$$c_i^k = \binom{2k}{i+2} (-1)^i (i+1)(i+2) \left(\left[S'(x)x^{2k-i-2} \right]_{-L/2}^{L/2} - (2k-i-2) \left[S(x)x^{2k-i-3} \right]_{-L/2}^{L/2} \right), \quad (28b)$$

$$c_{i,j}^k = \binom{i+j+4}{i} (-1)^i (i+1)(i+2)(j+1)(j+2). \quad (28c)$$

Transforming the operator of I_k in (23) by (27) and substituting equations (26), (28),

$$\begin{aligned} I_k &= c^k + \left(\sum_{i=k}^k + 2 \sum_{i=0}^{k-1} \right) \left(c_{2k-i-2}^k M_{2k-i-2} \right. \\ &\quad \left. + c_{i-2}^k M_{i-2} \right. \\ &\quad \left. + c_{i-2,2k-i-2}^k M_{i-2} M_{2k-i-2} \right) \\ &= c^k + \left(\sum_{i=k}^k + 2 \sum_{i=0}^{k-1} \right) \left(c_{2k-i-2}^k M_{2k-i-2} \right) \\ &\quad + \left(\sum_{i=k}^k + 2 \sum_{i=0}^{k-1} \right) \left(c_{i-2}^k M_{i-2} \right) \\ &\quad + \left(\sum_{i=k}^k + 2 \sum_{i=0}^{k-1} \right) \left(c_{i-2,2k-i-2}^k M_{i-2} M_{2k-i-2} \right) \\ &= c^k + c_{k-2}^k M_{k-2} + 2 \sum_{i=0}^{k-1} \left(c_{2k-i-2}^k M_{2k-i-2} \right) \\ &\quad + c_{k-2}^k M_{k-2} + 2 \sum_{i=0}^{k-1} \left(c_{i-2}^k M_{i-2} \right) \\ &\quad + c_{k-2,k-2}^k M_{k-2}^2 + 2 \sum_{i=0}^{k-1} \left(c_{i-2,2k-i-2}^k M_{i-2} M_{2k-i-2} \right). \end{aligned} \quad (29)$$

To proceed, we reverse the order in first sum that appears in (29) and change the indices in the second and third sum by $i \rightarrow i+2$ which transforms the summation limits to $\{-2, k-3\}$.

$$\begin{aligned} I_k &= c^k + c_{k-2}^k M_{k-2} + 2 \sum_{i=k-1}^{2k-2} \left(c_i^k M_i \right) \\ &\quad + c_{k-2}^k M_{k-2} + 2 \sum_{i=-2}^{k-3} \left(c_i^k M_i \right) \\ &\quad + c_{k-2,k-2}^k M_{k-2}^2 + 2 \sum_{i=-2}^{k-3} \left(c_{i,2k-i-4}^k M_i M_{2k-i-4} \right). \end{aligned} \quad (30)$$

Notice that in the last two sums, the terms for $i = \{-2, -1\}$ originate from II_0, II_1 respectively and can be set to zero. Then,

$$\begin{aligned}
I_k &= c^k + c_{k-2}^k M_{k-2} + 2 \sum_{i=k-1}^{2k-2} \binom{2k-2}{i} c_i^k M_i \\
&\quad + c_{k-2}^k M_{k-2} + 2 \sum_{i=0}^{k-3} \binom{k-3}{i} c_i^k M_i \\
&\quad + c_{k-2, k-2}^k M_{k-2}^2 + 2 \sum_{i=0}^{k-3} \binom{k-3}{i} c_{i, 2k-i-4}^k M_i M_{2k-i-4} \\
&= c^k \\
&\quad + 2 \sum_{i=0}^{2k-2} \binom{2k-2}{i} c_i^k M_i \\
&\quad + c_{k-2, k-2}^k M_{k-2}^2 + 2 \sum_{i=0}^{k-3} \binom{k-3}{i} c_{i, 2k-i-4}^k M_i M_{2k-i-4}.
\end{aligned} \tag{31}$$

Finally, looking at (20) and (31) we define the slender body operator \mathcal{G} of order n as,

$$\mathcal{G}(n) = \sum_{k=0}^n f(k; K) I_k, \tag{32}$$

which, under the assumption that the second derivative $S''(x)$ of the sectional area curve is bounded, will be a finite part of Vossers' integral. A proof for this statement is included in Appendix A

3.4 Sobol's Sensitivity Analysis

As stated earlier, in this section Sobol's methodology for SA is presented, it's sampling-based counterpart which can be used to approximate the relevant sensitivity indices is provided and the approach through which parameters are categorised as sensitive or insensitive is introduced. Let $X_i, i = \{1, \dots, n\}$ be the random input variables to the function $f : R^n \rightarrow R^k$, which produces the random vector $\mathbf{Y} = f(X_1, \dots, X_n) \in R^k$. Let \mathbf{u} be a non-empty r -subset of $\{1, \dots, n\}$ and let $\mathbf{X}_{\mathbf{u}} = (X_i, i \in \mathbf{u}) \in R^r$, $\mathbf{X}_{\bar{\mathbf{u}}} = (X_i, i \in \{1, \dots, n\}/\mathbf{u}) \in R^{n-r}$. Then, recall the Hoeffding decomposition [42] of f :

$$f(X_0, \dots, X_{n-1}) = c + f_{\mathbf{u}}(\mathbf{X}_{\mathbf{u}}) + f_{\bar{\mathbf{u}}}(\mathbf{X}_{\bar{\mathbf{u}}}) + f_{\mathbf{u}, \bar{\mathbf{u}}}(\mathbf{X}_{\mathbf{u}}, \mathbf{X}_{\bar{\mathbf{u}}}), \tag{33}$$

where $c \in R^k$, $f_{\mathbf{u}} : R^r \rightarrow R^k$, $f_{\bar{\mathbf{u}}} : R^{n-r} \rightarrow R^k$ and $f_{\mathbf{u}, \bar{\mathbf{u}}} : R^n \rightarrow R^k$ are given by:

$$c = E(\mathbf{Y}), \quad f_{\mathbf{u}} = E(\mathbf{Y} | \mathbf{X}_{\mathbf{u}}) - c, \quad f_{\bar{\mathbf{u}}} = E(\mathbf{Y} | \mathbf{X}_{\bar{\mathbf{u}}}) - c, \quad f_{\mathbf{u}, \bar{\mathbf{u}}} = \mathbf{Y} - f_{\mathbf{u}} - f_{\bar{\mathbf{u}}} - c. \tag{34}$$

Taking the covariance of (33), and due to L^2 -orthogonality:

$$Cov(f) = Cov(f_{\mathbf{u}}(\mathbf{X}_{\mathbf{u}})) + Cov(f_{\bar{\mathbf{u}}}(\mathbf{X}_{\bar{\mathbf{u}}})) + Cov(f_{\mathbf{u}, \bar{\mathbf{u}}}(\mathbf{X}_{\mathbf{u}}, \mathbf{X}_{\bar{\mathbf{u}}})) \tag{35}$$

Then to project these co-variances to a scalar, two approaches are to take the derivative or take the trace. The authors in [18], take the trace of these covariances and define the following three indices:

$$S^{\mathbf{u}}(f) = \frac{Trace(Cov(f_{\mathbf{u}}(\mathbf{X}_{\mathbf{u}})))}{Trace(Cov(f))}, \quad \text{sensitivity only to the inputs in } \mathbf{u} \tag{36a}$$

$$S^{\bar{\mathbf{u}}}(f) = \frac{Trace(Cov(f_{\bar{\mathbf{u}}}(\mathbf{X}_{\bar{\mathbf{u}}}))}{Trace(Cov(f))}, \quad \text{sensitivity only to the inputs not in } \mathbf{u} \tag{36b}$$

$$\begin{aligned}
S^{\mathbf{u}, \bar{\mathbf{u}}}(f) &= \frac{Trace(Cov(f_{\mathbf{u}, \bar{\mathbf{u}}}(\mathbf{X}_{\mathbf{u}}, \mathbf{X}_{\bar{\mathbf{u}}}))}{Trace(Cov(f))}, && \text{interaction between inputs of } \mathbf{u} \\
&&& \text{and inputs of } \{0, \dots, n-1\}/\mathbf{u}.
\end{aligned} \tag{36c}$$

Now, for $\mathbf{u} = \{i\}$, (36a) will be called the sensitivity index of the parameter c_i with respect to the quantity of interest f , and denoted as,

$$SI_i^f \equiv S^{\mathbf{u}}(f). \tag{37}$$

In accordance to [18], (37) can be approximated via a sampling-based algorithm. Specifically, first draw N independent samples $\mathbf{x}_i \in \mathbb{R}^n$, $i = 1, \dots, N$ from the entire design space which are sampled according to the respective probability density function ρ of the input parameters. Proceed by evaluating the respective responses $\mathbf{f}_i = f(\mathbf{x}_i)$. Then, for each \mathbf{x}_i , construct another sample \mathbf{x}_i^* by fixing c_i and only varying the rest of the parameters to evaluate $\mathbf{f}_i^* = f(\mathbf{x}_i^*)$. For $\mathbf{f}_i = (f_{i,1}, \dots, f_{i,k}) \in \mathbb{R}^k$, the sensitivity index SI_i^f of c_i is approximated by,

$$SI_i^f = \frac{\sum_{j=1}^k \left(\sum_{i=1}^N f_{i,j} f_{i,j}^* - \frac{1}{N} \left(\sum_{i=1}^N \frac{f_{i,j} + f_{i,j}^*}{2} \right)^2 \right)}{\sum_{j=1}^k \left(\sum_{i=1}^N \frac{(f_{i,j})^2 + (f_{i,j}^*)^2}{2} - \frac{1}{N} \left(\sum_{i=1}^N \frac{f_{i,j} + f_{i,j}^*}{2} \right)^2 \right)}. \quad (38)$$

Since in our case c_1, c_2, c_3 are design variables, ρ is chosen as the uniform PDF [14] so as not to introduce any bias towards any region of the design space. As stated earlier, each parameter c_i is characterised as sensitive or insensitive with respect to f by specifying a threshold value ϵ [19],

$$\begin{cases} SI_i^f > \epsilon \implies c_i \text{ sensitive parameter with respect to } f, \\ SI_i^f \leq \epsilon \implies c_i \text{ insensitive parameter with respect to } f. \end{cases} \quad (39)$$

In alignment with [12], ϵ has been chosen as 0.05 for this study.

3.5 Physics-Geometry Correlation Measures

Having evaluated the physics-based sensitivity indices $SI^{\mathcal{P}} = \{SI_1^{\mathcal{P}}, \dots, SI_n^{\mathcal{P}}\}$ and their geometry-based counterparts $SI^{\mathcal{G}} = \{SI_1^{\mathcal{G}}, \dots, SI_n^{\mathcal{G}}\}$ two metrics will be used to quantify their correlation,

$$\text{NRMSE} = \frac{\sqrt{\sum_{i=1}^n \frac{(SI_i^{\mathcal{P}} - SI_i^{\mathcal{G}})^2}{n}}}{\max(SI^{\mathcal{P}}) - \min(SI^{\mathcal{P}})}, \quad (40a)$$

$$\text{similarity} = \frac{\sum_{i=1}^n \overline{SI_i^{\mathcal{P}}} \cdot \overline{SI_i^{\mathcal{G}}}}{\sqrt{\sum_{i=1}^n \overline{SI_i^{\mathcal{P}}}} \sqrt{\sum_{i=1}^n \overline{SI_i^{\mathcal{G}}}}} \in [0, 1], \quad (40b)$$

where

$$\overline{SI_i^{\mathcal{P}}} = \begin{cases} 1, & SI_i^{\mathcal{P}} > \epsilon \\ 0, & \text{else} \end{cases}, \quad \overline{SI_i^{\mathcal{G}}} = \begin{cases} 1, & SI_i^{\mathcal{G}} > \epsilon \\ 0, & \text{else.} \end{cases} \quad (40c)$$

Equation (40a) is the Root Mean Square Error between $SI^{\mathcal{P}}$ and $SI^{\mathcal{G}}$ normalised by the former, while (40b) can be thought of as a discretised correlation between only the sensitive parameters of $SI^{\mathcal{P}}$ and $SI^{\mathcal{G}}$. More accurately, notice that if a parameter is insensitive in both $SI^{\mathcal{P}}$ and $SI^{\mathcal{G}}$ it then has no effect on (40b). However if a parameter is sensitive for one of $SI^{\mathcal{P}}, SI^{\mathcal{G}}$ but not the other, (40b) is penalised. This penalization can be interpreted as follows: if a parameter is sensitive for $SI^{\mathcal{P}}$ but not $SI^{\mathcal{G}}$ then the geometry-based DR has omitted important information regarding the relevant physics-based problem; if the opposite is true, then the geometry-based DR has not sufficiently reduced the dimensionality of the physics-based problem. These two metrics were used in [12] in an analogous context to this study.

4 Test Case: Wave Resistance and the Wigley-based Modeller

Looking at Figure 2, Section 3 was devoted to outlining two different choices of \mathcal{G} as well as the approach to dimensionality reduction and correlation analysis between the physics- and geometry-based sensitivity indices. This section introduces the chosen parametric modeller \mathcal{D}_1 and physics-based property \mathcal{P} .

4.1 Modified Wigley Hull Parametric Modeller

The modeller \mathcal{D} investigated in this study is a modified Wigley hull-form, a benchmark geometry which has been widely used in the literature [43]. The half-length and half-breadth subsurface of \mathcal{D} , is parameterised in 6 parameters $\{L, B, T, c_1, c_2, c_3\}$ and given by,

$$\mathcal{D}(\xi, \zeta; L, B, T, c_1, c_2, c_3) = \begin{bmatrix} \frac{L\xi}{2} \\ \frac{B\eta}{2} \\ T\zeta \end{bmatrix}, \quad \xi \in [0, 1], \zeta \in [0, 1], \quad (41a)$$

$$\eta = (1 - \zeta^2)(1 - \xi^2)(1 + c_1\xi^2 + c_2\xi^4) + c_3\zeta^2(1 - \zeta^8)(1 - \xi^2)^4, \quad (41b)$$

where L , B , T are the length breadth and draft respectively. While the effect of the first three parameters is clear, the same is not true for c_1 , c_2 and c_3 . Figures 3, 5 and 7 indicate this effect by varying each one between 0 and 1, while keeping the others fixed. Looking at the first two figures, note that c_1 and c_2 predominantly affect the deck area with negligible effect on the keel. By comparing Figures 3 and 5, which are identically scaled, it is easy to see that c_1 has a stronger effect on the deck when compared to c_2 . Varying c_3 mainly affects the keel of the hull, with no effect to the deck shape as is evident from the ζ^2 factor in (41). In Figure 7 one can see the transverse sections of the hull at midships ($\xi = 0$) for varying c_3 . Finally, the original Wigley hull is recovered by setting $c_1 = c_2 = c_3 = 0$.

It should be noted that if $S'(\pm L/2) \neq 0$, then (12) diverges [44], as is the case for the Wigley-hull family (41) where $S'(\pm L/2) = (8BT/3L)(1 + c_1 + c_2) \neq 0$ (see Appendix C). In this connection, we have adopted (13) as a finite part of (12).

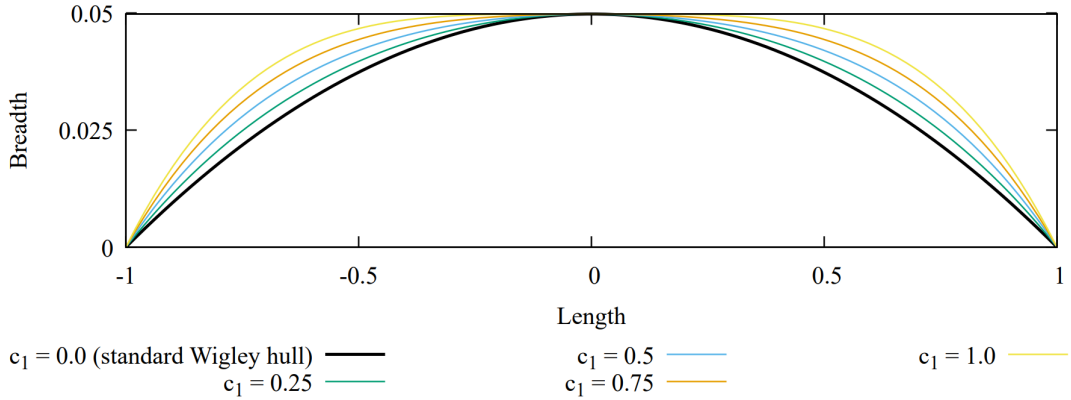


Figure 3: Effect of c_1 parameter on the modified Wigley hull. In this top-view figure, each curve is the deck-line corresponding to $c_1 = \{0.0, 0.25, 0.5, 0.75, 1.0\}$ with all other parameters fixed at $\{L = 1, B = 0.0996, T = 0.13775, c_2 = 0, c_3 = 0\}$.

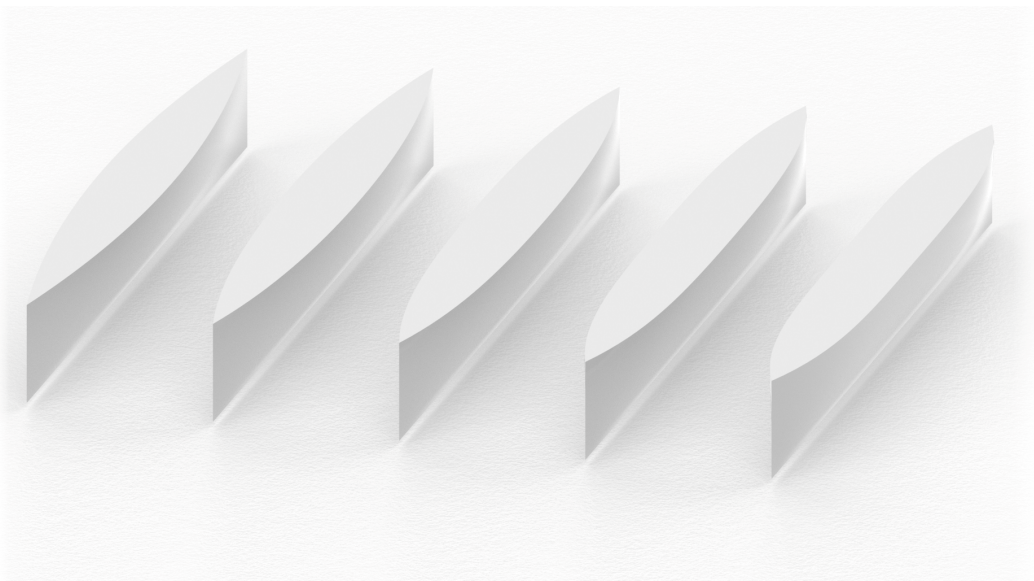


Figure 4: Renders of the modeller instances depicted in Figure 3. Specifically, from left to right, each hull corresponds to $c_1 = \{0.0, 0.25, 0.5, 0.75, 1.0\}$ with all other parameters fixed at $\{L = 1, B = 0.0996, T = 0.13775, c_2 = 0, c_3 = 0\}$.

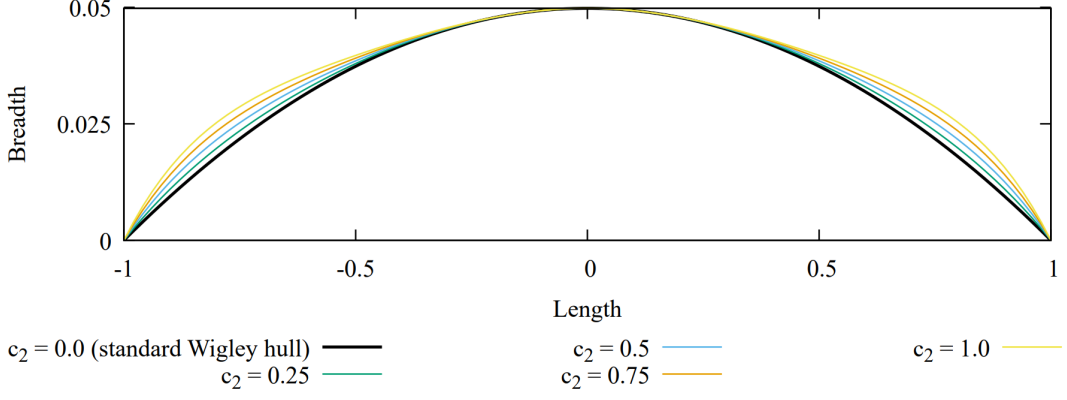


Figure 5: Effect of c_2 parameter on the modified Wigley hull. In this top-view figure, each curve is the deck-line corresponding to $c_2 = \{0.0, 0.25, 0.5, 0.75, 1.0\}$ with all other parameters fixed at $\{L = 1, B = 0.0996, T = 0.13775, c_1 = 0, c_3 = 0\}$.

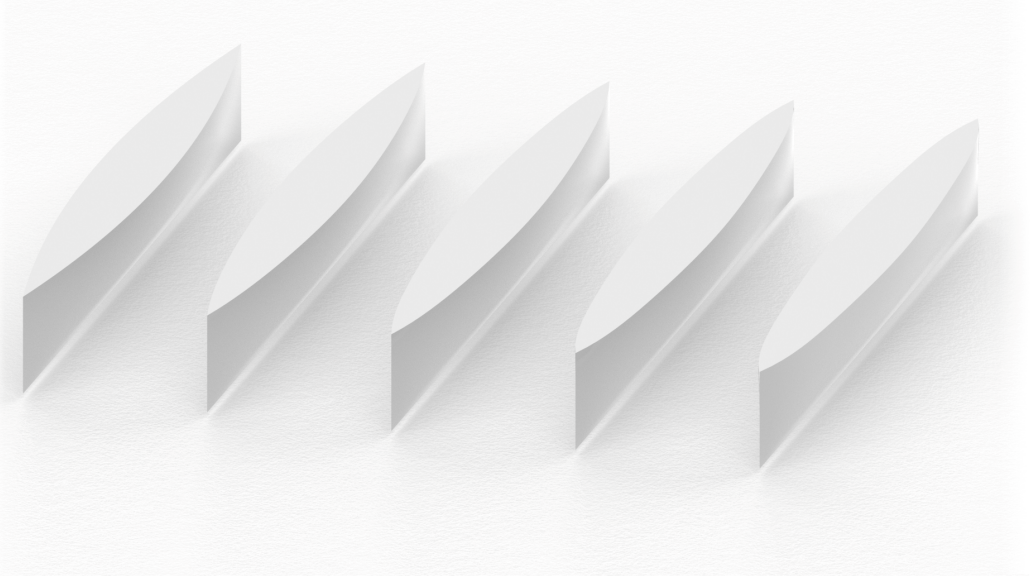


Figure 6: Renders of the modeller instances depicted in Figure 5. Specifically, from left to right, each hull corresponds to $c_2 = \{0.0, 0.25, 0.5, 0.75, 1.0\}$ with all other parameters fixed at $\{L = 1, B = 0.0996, T = 0.13775, c_1 = 0, c_3 = 0\}$.

4.1.1 Design Space Selection

The maximum number of parameters supported by (41) is 6, $\{L, B, T, c_1, c_2, c_3\}$. Similar to [12], a design space with uniform bounding box was chosen. We will now prove that this is indeed the case when L, B and T are fixed and $c_1 \times c_2 \times c_3 \in [0, 1]^3$. For fixed length, beam and draft, let \mathbf{S} be the three-parameter family of surfaces defined by

$$\mathbf{S}(\xi, \zeta; c_1, c_2, c_3) \equiv \mathcal{D}(\xi, \zeta; L, B, T, c_1, c_2, c_3). \quad (42a)$$

If S_i is the i^{th} coordinate function of \mathbf{S} , define the bounding box of \mathbf{S} for a given choice of c_1, c_2, c_3 as

$$\mathcal{B}(c_1, c_2, c_3) = \{\mathbf{p} = (p_1, p_2, p_3)^T \in \mathbb{R}^3 : \min_{D_{\mathbf{S}}} S_i \leq p_i \leq \max_{D_{\mathbf{S}}} S_i, \quad i = 1, 2, 3\}, \quad (42b)$$

where $D_{\mathbf{S}} = [0, 1]^2$ is the domain of \mathbf{S} . We will show that $\mathcal{B}(\cdot, \cdot, \cdot)$ is constant. Looking at (41), it is evident that for $i = 1, 3$ the minimum/maximum values of S_i are taken at $\xi = \zeta = 0 / \xi = \zeta = 1$ respectively and are independent to c_1, c_2, c_3 . For $i = 2$ it is enough to show that $\min_{D_{\mathbf{S}}} \eta$ and $\max_{D_{\mathbf{S}}} \eta$ are independent to these three parameters as well. One can easily verify that in $D_{\mathbf{S}}$, $\eta \geq 0$ and $\eta(\xi, 1; c_1, c_2, c_3) = 0$. Therefore, $\min_{D_{\mathbf{S}}} \eta = 0$ which is independent to c_1, c_2 and c_3 . For the maximum of η notice that for $0 \leq c_i \leq 1$,

$$\begin{aligned} 0 &\leq (1 - \zeta^2)(1 - \xi^2)(1 + c_1\xi^2 + c_2\xi^4) \leq (1 - \zeta^2)(1 - \xi^2)(1 + \xi^2 + \xi^4) \\ &0 \leq c_3\zeta^2(1 - \zeta^8)(1 - \xi^2)^4 \leq \zeta^2(1 - \zeta^8)(1 - \xi^2)^4. \end{aligned}$$

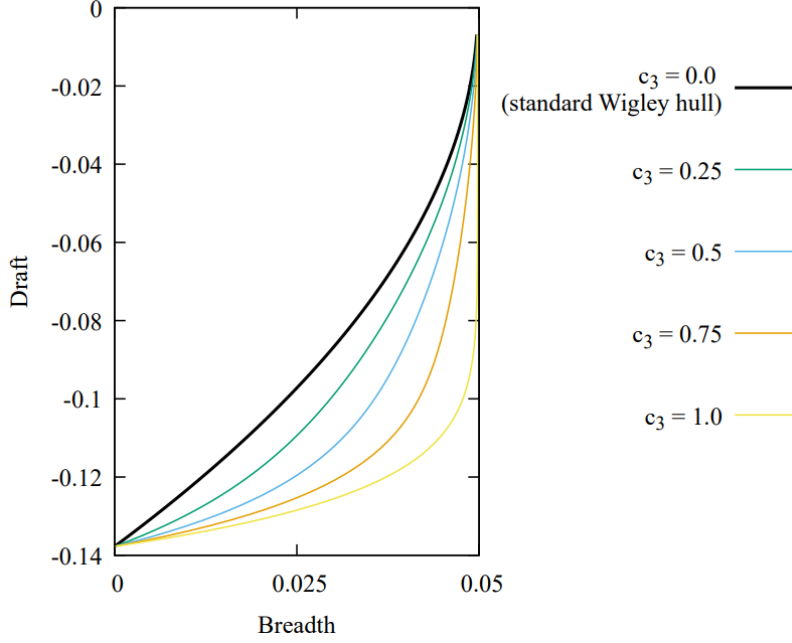


Figure 7: Effect of c_3 parameter on the modified Wigley hull. In this front-view figure, each curve is the depth-line corresponding to $c_3 = \{0.0, 0.25, 0.5, 0.75, 1.0\}$ with all other parameters fixed at $\{L = 1, B = 0.0996, T = 0.13775, c_1 = 0, c_2 = 0\}$.

Adding the two inequalities yields

$$\eta(\xi, \zeta; c_1, c_2, c_3) \leq \eta(\xi, \zeta; 1, 1, 1), \quad \xi \times \zeta \times c_1 \times c_2 \times c_3 = [0, 1]^5, \quad (42c)$$

where $\eta(\xi, \zeta; 1, 1, 1)$ is clearly independent to c_1, c_2 and c_3 . We complete this proof by showing that $\max_{D_S} \eta(\xi, \zeta; c_1, c_2, c_3) = \max_{D_S} \eta(\xi, \zeta; 1, 1, 1)$ for any c_1, c_2 and c_3 . Denote $g(\xi, \zeta) = \eta(\xi, \zeta; 1, 1, 1)$ with $D_g = [0, 1]^2$. Since g is differentiable, if $g(\xi^*, \zeta^*)$ is a maximum, then either (ξ^*, ζ^*) is a singular point and/or it is on the boundary of D_g . We begin by investigating the first case,

$$\begin{aligned} \frac{\partial g}{\partial \xi} &= -2\xi(1 - \zeta^2)(1 + \xi^2 + \xi^4) + (1 - \zeta^2)(1 - \xi^2)(2\xi + 4\xi^3) + \zeta^2(1 - \zeta^8)4(1 - \xi^2)^3(-2\xi) \\ &= 2\xi(1 - \zeta^2) \left(-(1 + \xi^2 + \xi^4) + (1 - \xi^2)(1 + 2\xi^2) - \zeta^2(1 + \zeta^2)(1 + \zeta^4)4(1 - \xi^2)^3 \right) \\ &= 2\xi(1 - \zeta^2) \left(-1 - \xi^2 - \xi^4 + 1 + 2\xi^2 - \xi^2 - 2\xi^4 - \zeta^2(1 + \zeta^2)(1 + \zeta^4)4(1 - \xi^2)^3 \right) \\ &= 2\xi(1 - \zeta^2) \left(-3\xi^4 - \zeta^2(1 + \zeta^2)(1 + \zeta^4)4(1 - \xi^2)^3 \right). \end{aligned} \quad (42d)$$

When not in the boundary of D_g such that $\xi, \zeta \in (0, 1)$ it is evident from (42d) that $\partial g / \partial \xi < 0$ and therefore, there are no singular points in the interior of D_g . For the second case where $(\xi, \zeta) \in \text{Bd}(D_g)$,

$$g(\text{Bd}(D_g)) = \left\{ \begin{array}{ll} 0 & , \quad (\xi, \zeta) = (1, \zeta) \text{ or } (\xi, 1) \\ 1 - \zeta^8 & , \quad (\xi, \zeta) = (0, \zeta) \\ 1 - \xi^6 & , \quad (\xi, \zeta) = (\xi, 0) \end{array} \right\}. \quad (42e)$$

Then $\max_{\text{Bd}(D_g)} g = 1$ and further, by the non-singularity of g in $\text{Int}(D_g)$, it follows that $\max_{D_g} g = \max_{\text{Bd}(D_g)} g = 1$. All that is left now is to show that $\max_{D_S} \eta(\xi, \zeta; c_1, c_2, c_3) = \max_{D_S} \eta(\xi, \zeta; 1, 1, 1) \stackrel{\text{def}}{=} \max_{D_g} g(\xi, \zeta) = 1$ for any c_1, c_2 and c_3 . By (42c) it is sufficient to show that there exist ξ^* and ζ^* such that $\eta(\xi^*, \zeta^*; c_1, c_2, c_3) = 1$. Indeed, substitute $(\xi^*, \zeta^*) = (0, 1)$ in equation (41) to verify this statement and complete the proof.

4.1.2 Closed Forms of the Geometric Moments of the Modified Wigley Hull

Due to the simple analytical expression (41) of the modified Wigley hull, it is possible to evaluate the moments (8) analytically with the relevant analysis carried out in Appendix B. Specifically, $M(p, q, r)$ and $M_T(p, q, r)$ are given in equations (68) and (72) respectively, while $M_S(p, q, r)$ and $M_I(p, q, r)$ can easily be computed using (7) and (8)



Figure 8: Renders of the modeller instances depicted in Figure 7. Specifically, from left to right, each hull corresponds to $c_3 = \{0.0, 0.25, 0.5, 0.75, 1.0\}$ with all other parameters fixed at $\{L = 1, B = 0.0996, T = 0.13775, c_1 = 0, c_2 = 0\}$.

4.2 Wave Resistance Coefficient

In line with [12], \mathcal{P} is identified with the wave resistance coefficient, C_w . This choice can be attributed to its explicit connection to the SAC, $S(x)$, of a hull which is a purely geometric property. This connection was initially established in the context of slender body theory via the so called Vossers' integral [41] as in equation (12). Further development continued ([45]; [46]; [47]) which, however, resulted in a theory suffering from a number of deficiencies as pointed out in [48] and [44]. Nevertheless, the SAC's importance in resistance-related ship-design problems which originated by the so-called Lackenby transformation [49] has continued till recent times ([21]; [50])

The C_w of (41) was approximated using a Boundary Element Method-based solver in the context of IsoGeometric Analysis (IGA-BEM), as introduced in [51]. To utilise this solver, the input geometry must be provided in B-spline form, which is not the case for (41). However, it is important to note that (41) represents a polynomial surface of degree 8 in ξ and 10 in ζ . This means that only a change from the monomial to the B-spline basis is necessary or rather to the simpler Bernstein basis, needing only a single 8×10 patch for the surface to be explicitly represented. The resulting Bezier surface will be represented by $(8+1)(10+1) = 99$ control points $\mathbf{b}_{i,j}$, $i = 0, \dots, 8$, $j = 0, \dots, 10$ which are calculated numerically: for $B_{n,i}$ the Bernstein polynomial of degree n , find $\mathbf{b}_{i,j}$ such that for $\mathcal{D} : [0, 1]^2 \rightarrow \mathbb{R}^3$ the wiggly hull presented in (41) it is true that

$$\mathcal{D}(\xi, \zeta) = \sum_{i=0}^8 \sum_{j=0}^{10} B_{8,i}(\xi) B_{10,j}(\zeta) \mathbf{b}_{i,j}, \quad \xi \times \zeta \in [0, 1]^2. \quad (43)$$

To find the control points in (43) it is enough to evaluate \mathcal{D} at 99 distinct points in $[0, 1]^2$, $\mathbf{p}_{i,j}$ so that (43) is converted to three linear systems (one for each coordinate of $\mathbf{b}_{i,j}$) each of 99 independent equations in 99 unknowns. Finally, the choice of $\mathbf{p}_{i,j}$ was done uniformly in ξ , ζ ,

$$\mathbf{p}_{i,j} = (i/8, j/10), \quad i = 0, \dots, 8, \quad j = 0, \dots, 10. \quad (44)$$

Having found $\mathbf{b}_{i,j}$ it was then straightforward to supply the relevant knot sequences such that the resulting Bezier surface can be interpreted as a B-spline patch.

5 Results and Discussion

This section presents the detailed numerical results of the methodology outlined in Figure 2 both for SSV- and slender body (\mathcal{G})-based geometric operators, presented in Sections 3.2 and 3.3, respectively. The approximation of the relevant sensitivity indices is carried out using a sampling-based strategy. This implies the necessity of selecting a sampling strategy and analysing the computed approximation (38) for convergence.

The chosen sampling strategy is detailed in Section 5.1, while its convergence in case of wave resistance, SSV- and G-based geometric operators is presented in Sections 5.2, 5.3, and 5.4, respectively. Finally, in Section 5.5, all the aforementioned results are summarised. Correlation measures (40a) and (40b) are applied to the computed indices to compare the performance of SSV versus that of the slender body operator.

5.1 Dynamic Propagation Sampling

The choice of sampling algorithm is of fundamental importance to the expedited convergence of (38), therefore, a Dynamic Propagation Sampling (DPS) [8] is utilised in this study. The principal idea behind DPS is an optimisation based approach, which aims at creating uniformly distributed and diverse number of sample over multiple run. DPS achieves this while minimising an objective function, which is a weighted combination of three sampling criteria; **space-filling**, **non-collapsing** and **repulsion**.

Given a sample-set of N samples, $\mathbf{S}_N = \{\mathbf{s}_i, i = 1, \dots, N\}$, $\mathbf{s}_i \in \mathbb{R}^n$ the space-filling criterion ensures that the samples \mathbf{s}_i are uniformly distributed over the entire design space. This criterion is defined as $f_1 : (\mathbb{R}^n)^N \rightarrow \mathbb{R}$

$$f_1(\mathbf{S}_N) = \sum_{i=1}^{N-1} \sum_{j=i+1}^N \frac{1}{\|\mathbf{s}_i - \mathbf{s}_j\|^2}, \quad (45)$$

where $\|\cdot\|$ is the Euclidean norm in \mathbb{R}^k . However, minimisation of f_1 tends to place samples towards the boundary of the design space. To address this issue, the non-collapsing criterion is introduced through the discretisation of the design space into N^k disjoint subsets and the construction of a functional that discourages samples from being in the same subset. Specifically, if the range of each parameter $c_i \in [a_i, b_i]$ is divided into N sub-intervals $a_i = t_i^0 < t_i^1 < \dots < t_i^N = b_i$ define the discrete position $\mathbf{d}_s \in \mathbb{R}^n$ of a sample $\mathbf{s} \in \mathbb{R}^n$ as,

$$\mathbf{d}_s = [d_1, \dots, d_N], \quad \text{such that } \forall i, \quad \mathbf{s}_i \in [t_i^{d_i}, t_i^{d_i+1}). \quad (46a)$$

Then, the related functional is defined as,

$$f_2(\mathbf{S}_N) = \omega \sum_{i=1}^{N-1} \sum_{j=i+1}^N \mathcal{K}(\mathbf{s}_i, \mathbf{s}_j), \quad (46b)$$

$$\mathcal{K}(\mathbf{s}_i, \mathbf{s}_j) = \sum_{m=1}^n \delta\left(\left(\mathbf{d}_{\mathbf{s}_i}\right)_m, \left(\mathbf{d}_{\mathbf{s}_j}\right)_m\right), \quad (46c)$$

where ω is a user-controlled weight on the non-collapsing criterion, $(\mathbf{d}_s)_m$ is the m^{th} element of the discrete position of \mathbf{s} and $\delta(i, j)$ is Kronecker's delta.

Finally, DPS can be used to create a new set of samples, while ensuring that they are different from the previous sampled samples. Given an already existent sample set of M samples $\hat{\mathbf{S}}_M = \{\hat{\mathbf{s}}_i, i = 1, \dots, M\}$ DPS uses the repulsion criterion (f_3) to ensure that the new samples \mathbf{S}_N are different from the previous sampled designs. The formulation of f_3 is similar to that of f_1 ,

$$f_3(\mathbf{S}_N) = \sum_{i=1}^N \sum_{j=1}^M \frac{1}{\|\mathbf{s}_i - \hat{\mathbf{s}}_j\|^2}, \quad (47)$$

where $\|\cdot\|$ is the Euclidean norm in \mathbb{R}^k . Finally, define $f(\mathbf{S}_N) = f_1(\mathbf{S}_N) + f_2(\mathbf{S}_N) + f_3(\mathbf{S}_N)$ as the functional to be minimised.

5.2 C_w based SA

In order to identify the number of samples N to use for the reliable implementation of (38) the relevant convergence has to be investigated. Figure 9 show the sensitivity indices of the parameters with respect to C_w over the varying number of samples. Evaluation of sensitivity indices commenced with 10 samples and varied to 350 samples. It can be seen that sensitivity indices are unstable until 100 samples, however, they tend to converge afterwording, indicating that c_1 , c_2 are sensitive parameters while c_3 is an insensitive parameter. This is to be expected due to the nature of the wave-making phenomenon: due to the wave effect exponential decaying with respect to depth, c_3 which as shown in Figure (7) predominantly affects the keel of the hull, is expected to have less of an effect on C_w when compared to c_1 , c_2 which predominantly affect the deck. Moreover, notice that the effect of c_1 on C_w is significantly greater than that of c_2 which can be again justified by comparing Figures 3 and 5: the c_1 parameter has a significantly greater effect on the deck-geometry, compared to c_2 .

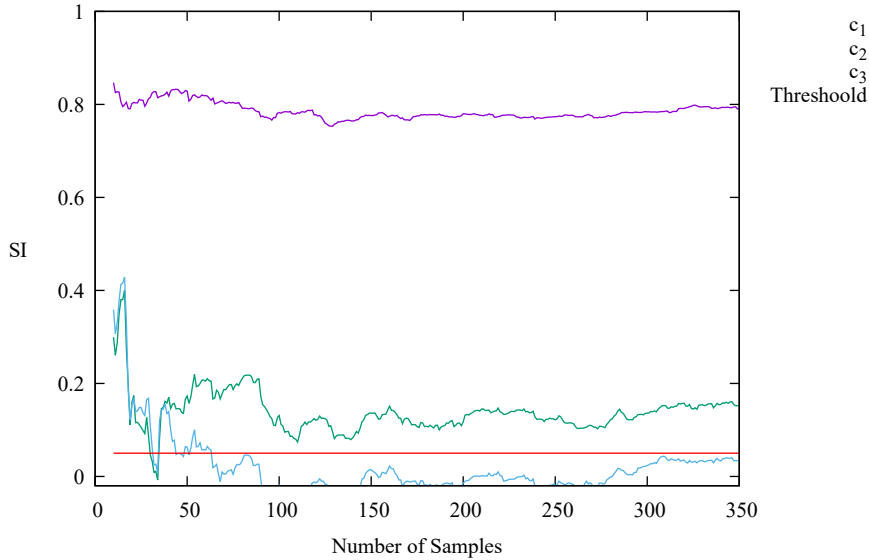


Figure 9: Convergence of C_w -based sensitivity indices. The horizontal axis is the number of DPS-generated samples while the vertical axis shows the sensitivity indices (SI)

5.3 SSV based SA

In contrast to the C_w -based SA, performing sensitivity analysis with respect to SSV necessitates the choice of a right order n . In [12], the authors investigated up to $n = 4$, as high-order geometric moments can be sensitive to noise while at the same time, numerical inaccuracies are ever-present when evaluating high-order terms. However, due to the simple expression of (41), the evaluation of high-order moments is computationally inexpensive and less prone to noise and inaccuracies. Therefore, in this study, the chosen range of n is $\{2, \dots, 15\}$. Consequently, each order n will yield its respective parameter sensitivity indices, necessitating a convergence analysis for all orders and parameters. This results in a total of 42 distinct convergence graphs, which can be found in Figures 10 through 12. Each graph corresponds to one of the three parameters: c_1 , c_2 , and c_3 .

Several noteworthy observations should be made about these results. Firstly, it is apparent that the number of samples required for convergence is significantly higher compared to C_w in Figure 9. This disparity can be attributed to certain sensitivity indices being closer to the threshold value set at 0.05. Additionally, indices evaluated with respect to higher-order SSVs tend to exhibit greater stability with regard to the number of samples. In other words, they require fewer samples to achieve convergence compared to lower-order SSVs. This trend is particularly evident in parameters c_1 and c_2 , which were sensitive to C_w . Moreover, note the similarity in sensitivity indices related to consecutive orders of the form $2k$ and $2k + 1$. This behaviour can be attributed to the length and breadth-wise symmetry of the Wigley hull (41), resulting in the vanishing of odd-index moments in their first and/or second positions, as seen in (68).

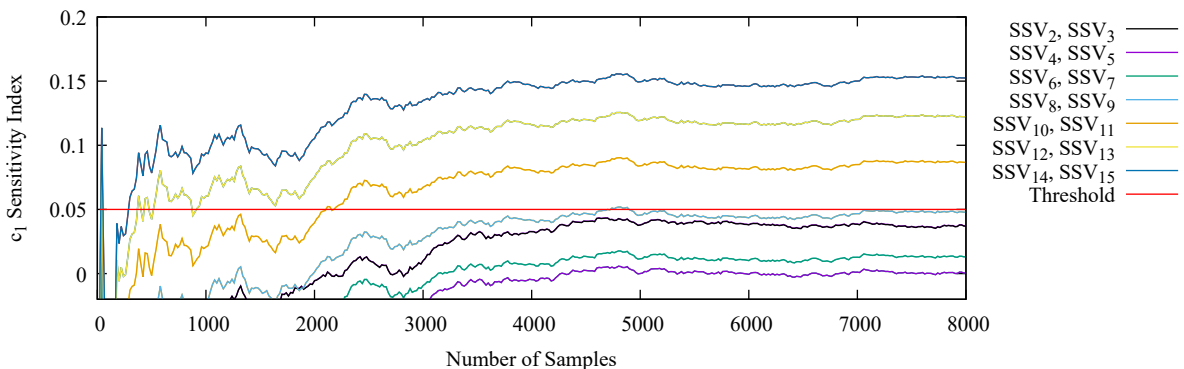


Figure 10: Convergence of the SSV-based sensitivity index of parameter c_1 with respect to the number of samples across varying order from 2 to 15.

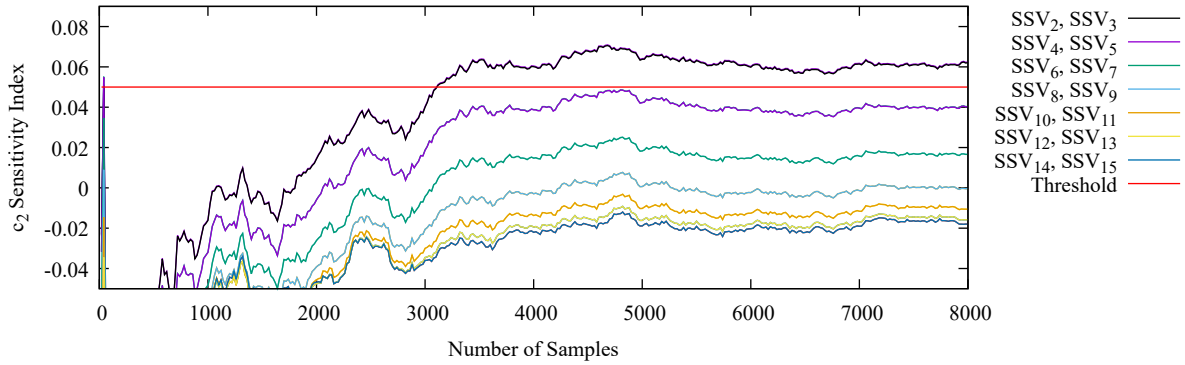


Figure 11: Convergence of the SSV-based sensitivity index of parameter c_2 with respect to the number of samples across varying order from 2 to 15.

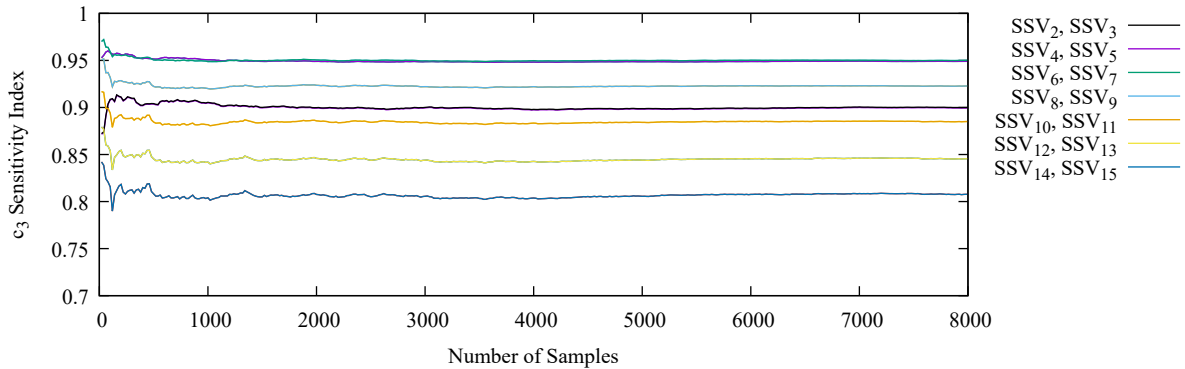


Figure 12: Convergence of the SSV-based sensitivity index of parameter c_3 with respect to the number of samples across varying order from 2 to 15.

Figures 13 through 15 show the comparative results of sensitivity indices with respect to SSV and C_w , where each figure is related to one of the parameters. In the case of parameter c_1 , which is clearly sensitive to C_w , its sensitivity index increases with the order n of SSV. Interestingly, it is insensitive until SSV₇ and then tends to increase steadily. However, in Figure 14, c_2 indicates a behaviour opposite to c_1 , i.e., its sensitivity reduces as the order of SSV increases. Based on the threshold of 0.05, it tends to be sensitive up to SSV₅. Note that in Figure 14, some of the indices are negative, indicating convergence, but some are numerically zero. Since their confidence intervals include zero, we can safely treat them as zero. Finally, in the case of c_3 , SSV _{n} and C_w are in complete disagreement, with this parameter being insensitive to C_w while highly sensitive to SSV _{n} . This misalignment in the c_3 highlights one of the shortcomings of SSV—its inability to differentiate between keel-wise and deck-wise changes to the geometry, which are crucial for wave-making.

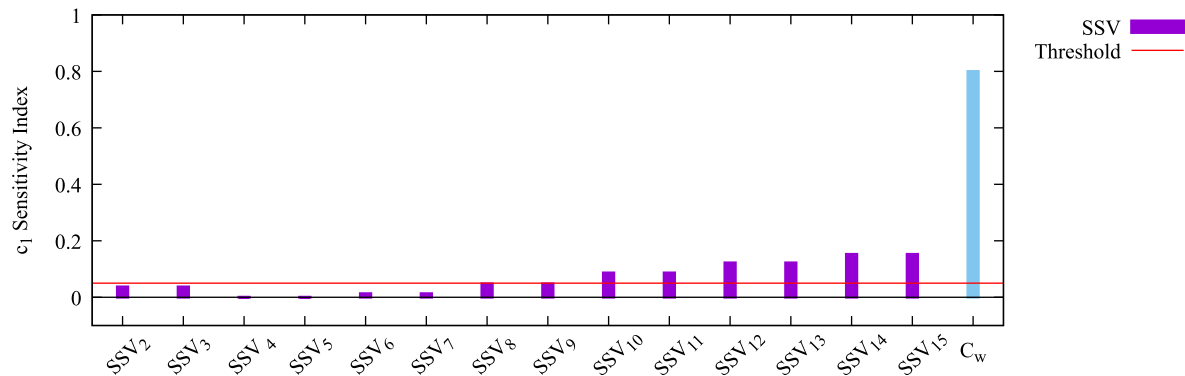


Figure 13: C_w - and SSV-based sensitivity indices of parameter c_2 evaluated with 8000 samples over SSV orders varying from 2 to 15.

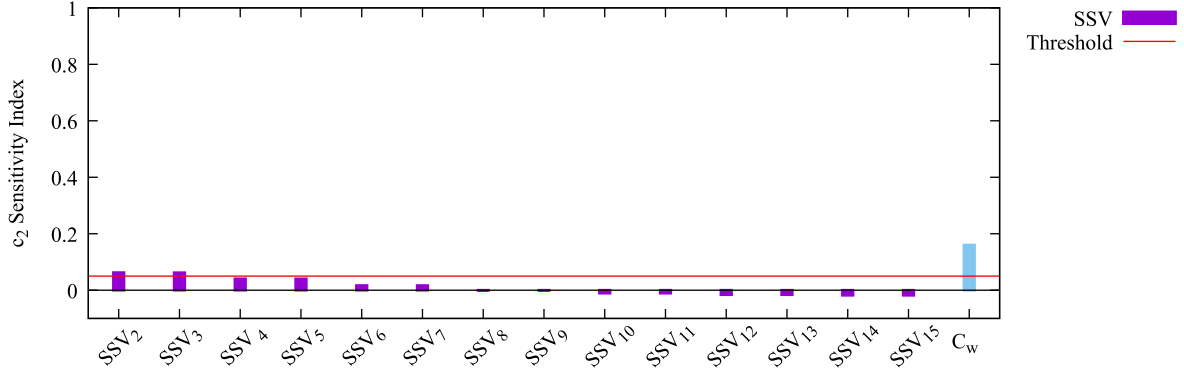


Figure 14: C_w - and SSV-based sensitivity indices of parameter c_2 evaluated with 8000 samples over SSV orders varying from 2 to 15.

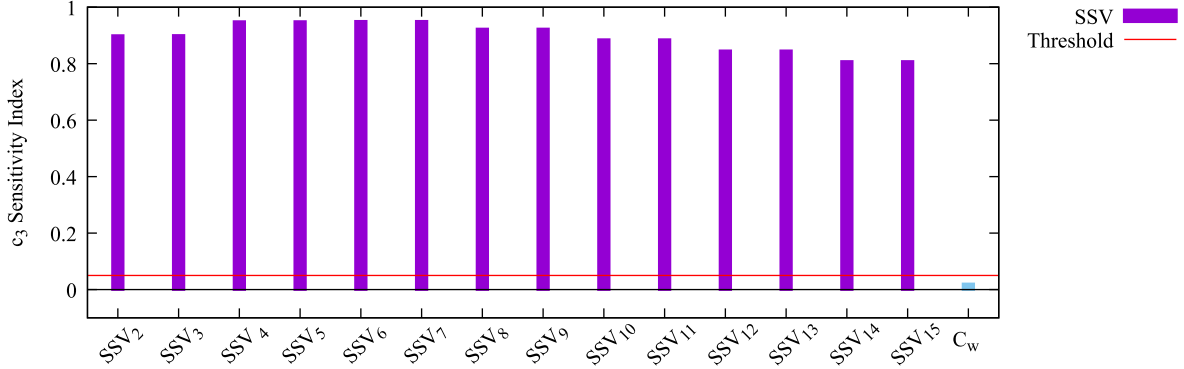


Figure 15: C_w - and SSV-based sensitivity indices of parameter c_2 evaluated with 8000 samples over SSV orders varying from 2 to 15.

5.4 Slender Body Operator based SA

Considering (58) and in contrast to the SSV-based sensitivity analysis, it would not yield meaningful results to the reader by deriving outcomes for a range of orders n as depicted in Figures 10 through 15. This would unnecessarily lengthen the paper. Instead, it is more reasonable to identify a singular sufficiently high n where the corresponding sensitivity indices have reached convergence. To ensure the convergence of (38) concerning both the sample size and the order n . These two variables are incrementally adjusted in the following manner: for each order n , the necessary sample size to guarantee the convergence of $\mathcal{G}(n)$ is determined before examining whether the consecutive differences $|\mathcal{G}(k+1) - \mathcal{G}(k)|$ have sufficiently diminished. Figures 16 through 18 depict the \mathcal{G} -based sensitivity indices c_1 , c_2 , and c_3 respectively, as the sample size increases for \mathcal{G} -orders ranging from 0 to 15.

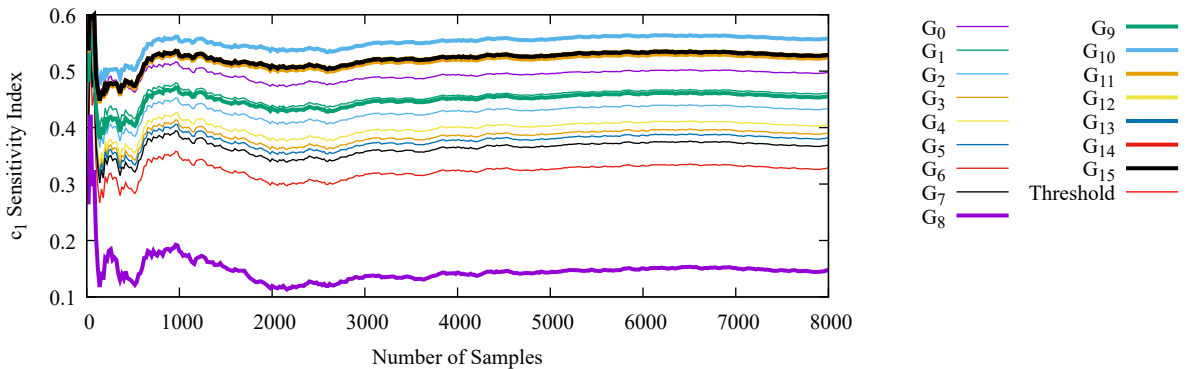


Figure 16: Convergence of the \mathcal{G} -based sensitivity index of parameter c_1 with respect to the number of samples across different orders of \mathcal{G} .

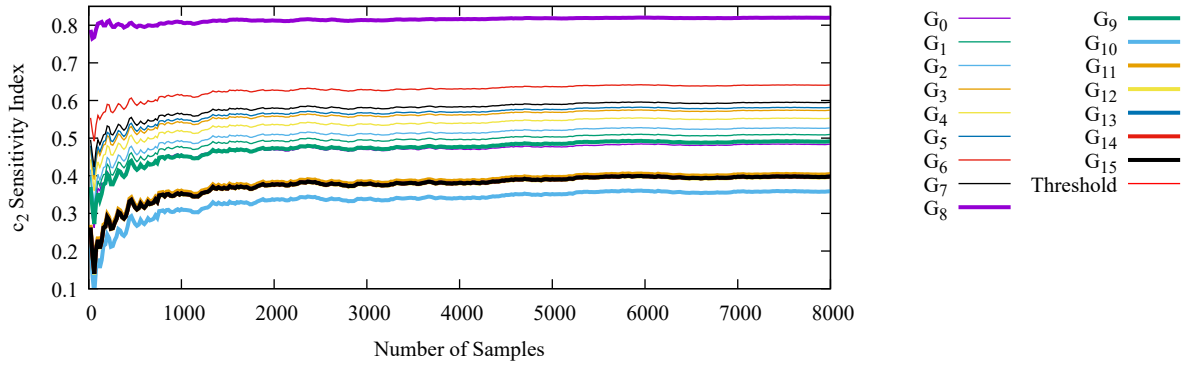


Figure 17: Convergence of the \mathcal{G} -based sensitivity index of parameter c_2 with respect to the number of samples across different orders of \mathcal{G} .

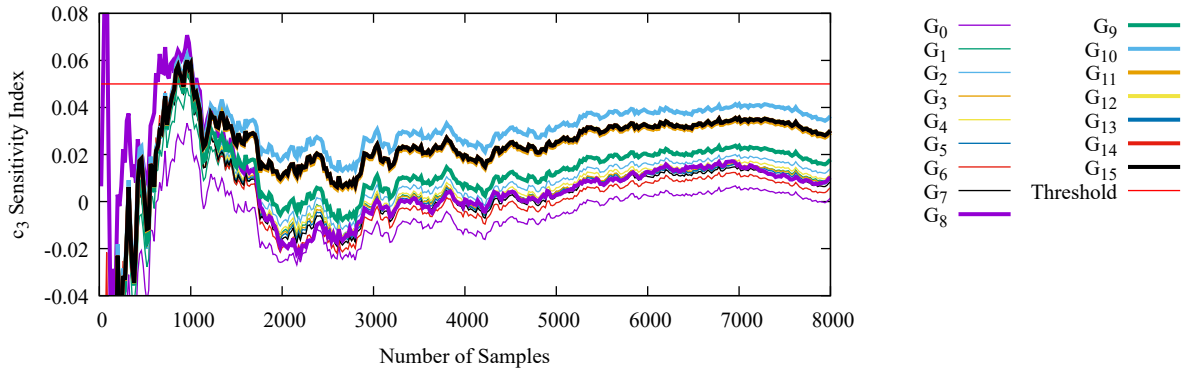


Figure 18: Convergence of the \mathcal{G} -based sensitivity index of parameter c_3 with respect to the number of samples across different orders of \mathcal{G} .

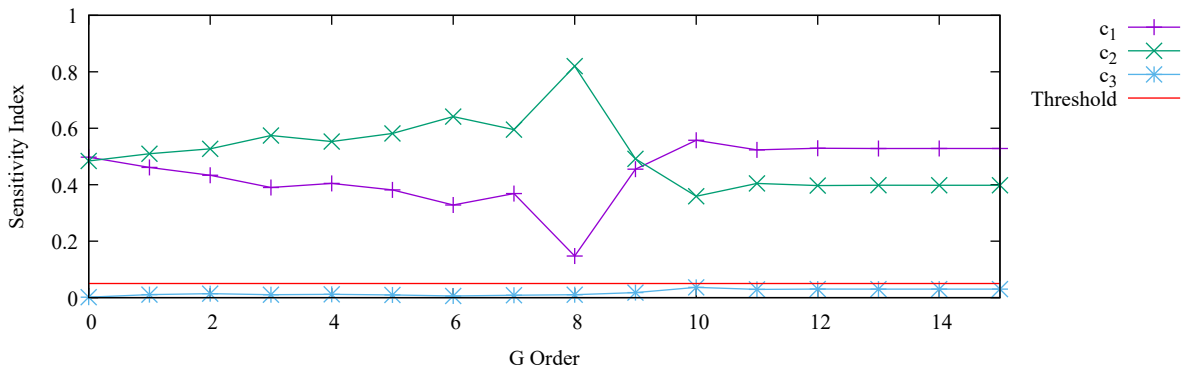


Figure 19: Convergence of \mathcal{G} -based sensitivity indices with respect to order from 0 to 15 at 8000 samples.

Notice in Figures 16 through 18 that the graphs of \mathcal{G}_{12} , \mathcal{G}_{13} , \mathcal{G}_{14} , and \mathcal{G}_{15} are practically identical, providing evidence for the validity of (58). To better illustrate this, sensitivity indices for all parameters and orders were retrieved at 8000 samples from Figures 16, 17, and 18 and replotted, this time with the \mathcal{G} orders on the horizontal axis (see Figure 19). Evidently, for orders greater than 11, the sensitivity indices for c_1 , c_2 , and c_3 show negligible variation.

Further insights were gained by retrieving the sensitivity indices of the three parameters at order 15 and plotting them in comparison to their C_w -based counterparts (see Figure 20). The results indicate agreement between \mathcal{G} and C_w with respect to the threshold. Additionally, the relative importance of c_1 , c_2 , and c_3 is maintained during the transition between C_w and \mathcal{G} . In both cases, it holds true that $SI_{c_1} > SI_{c_2} > SI_{c_3}$.

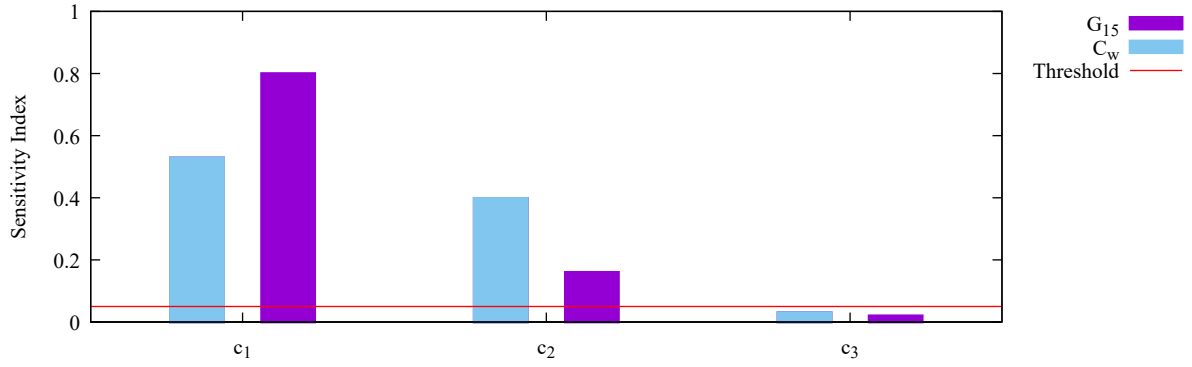


Figure 20: \mathcal{G}_{15} -based sensitivity indices comparison to C_w -based sensitivity indices at 8000 samples

5.5 Summary of SA Results

The resulting sensitivity indices with respect to SSV, \mathcal{G} , and C_w for parameters c_1 , c_2 , and c_3 are summarized in Figures 21, 22, and 23, respectively. Notice that in all figures, the behaviour of \mathcal{G}_{15} is significantly more aligned with C_w compared to that of SSV_n , especially in the case of c_3 .

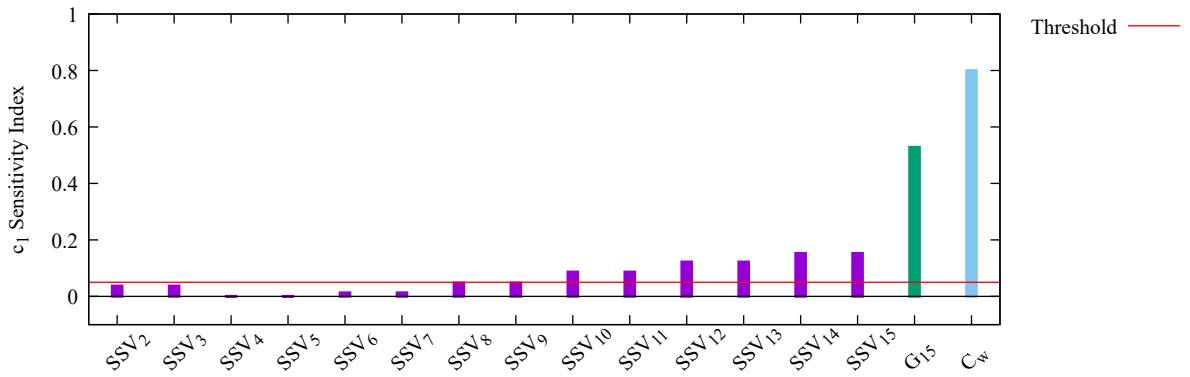


Figure 21: Sensitivity indices of c_1 parameter based on SSV of orders varying from 2 to 15, \mathcal{G} of order 15, and C_w

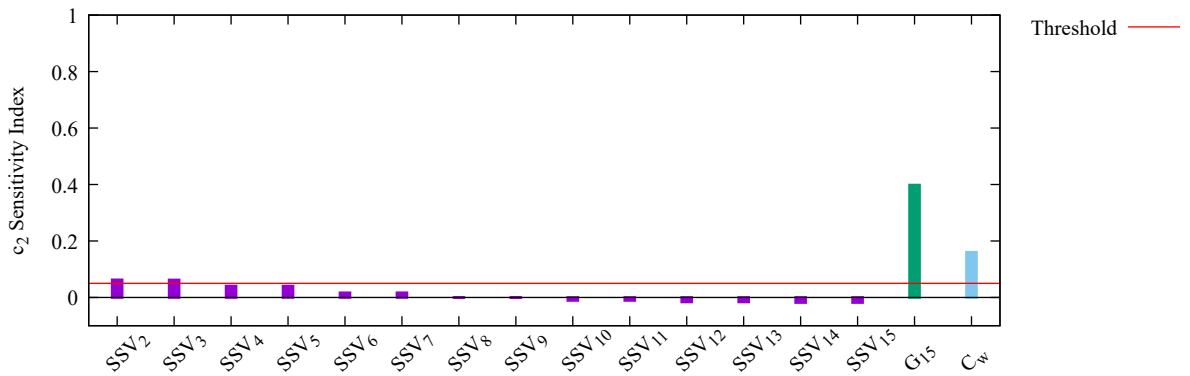


Figure 22: Sensitivity indices of c_2 parameter based on SSV of orders varying from 2 to 15, \mathcal{G} of order 15, and C_w

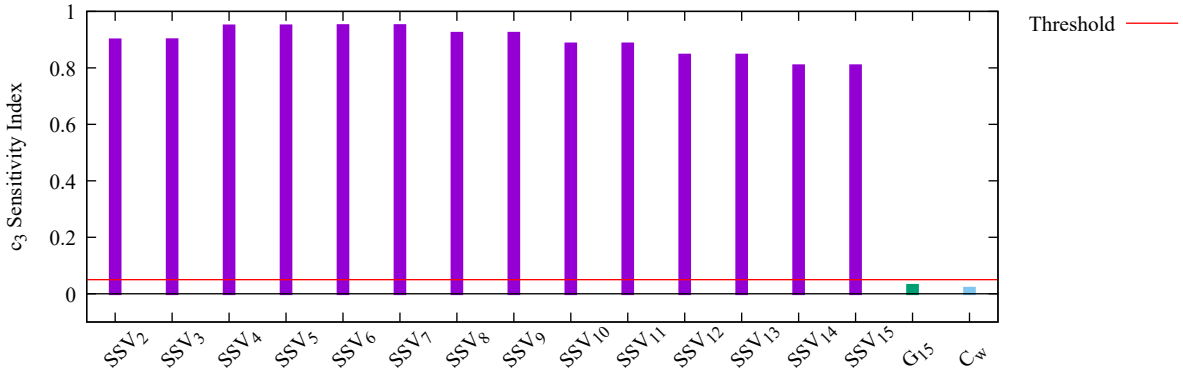


Figure 23: Sensitivity indices of c_3 parameter based on SSV of orders varying from 2 to 15, \mathcal{G} of order 15, and C_w .

The correlation measures (40a) and (40b) can be applied to Figures 21 through 23 so that the performance of SSV relative to that of \mathcal{G} can be more easily compared. Doing so for (40a) and (40b) results in Figures 24 and 25, respectively. Notice in Figure 25 that the slender body operator \mathcal{G}_{15} is able to capture 100% of the sensitive parameters.

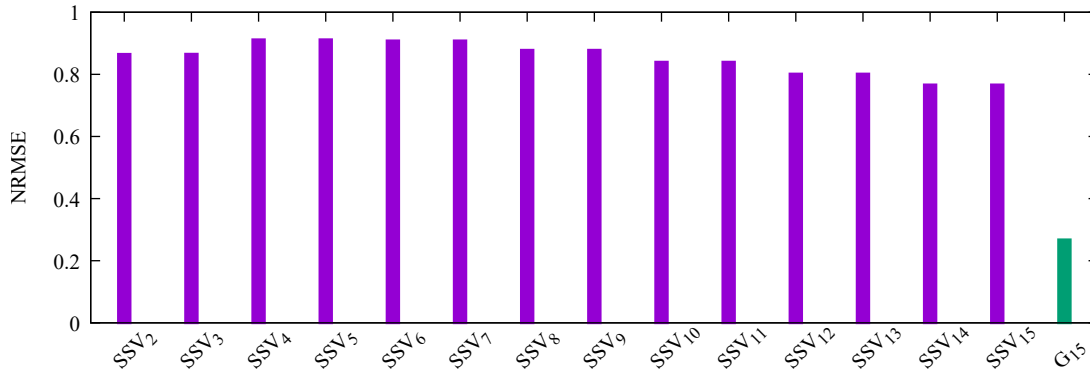


Figure 24: Error (40a) between SSV- and C_w -based sensitivity indices compared to error between \mathcal{G} -based and C_w -based sensitivity indices.

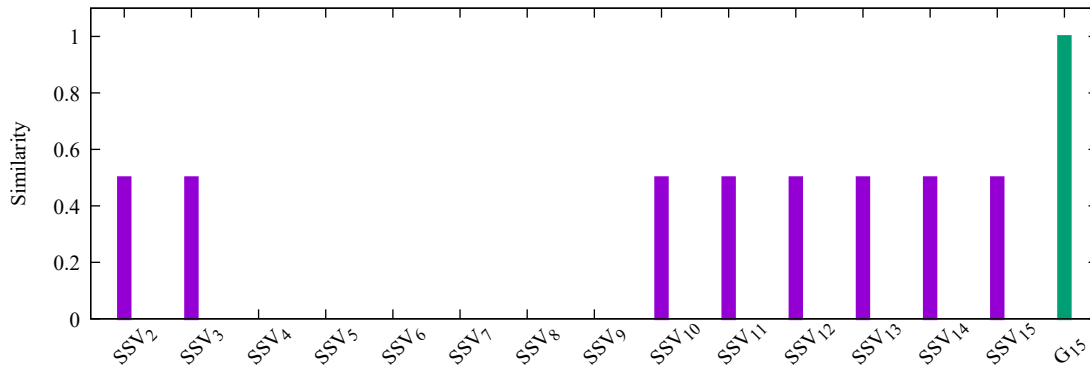


Figure 25: Similarity (40b) between SSV- and C_w -based sensitivity indices compared to similarity between \mathcal{G} - and C_w -based sensitivity indices.

Next, in Table 1, one can identify the sensitive parameters from Figures 21, 22, 23, in order of importance, as well as the normalised error and percentage similarity from Figures 24 and 25. Notice that not only does \mathcal{G}_{15} outperform SSV_n in terms of error (40a) and similarity (40b), but also the relative importance of the parameters is preserved, so that c_1 can be correctly identified as more influential than c_2 . These results illustrate that the inclusion of additional information regarding the underlying geometry with the SSV_n operators, in contrast to the restriction to moments of the form $M(N, 0, 0)$, as is the case with \mathcal{G} , produces results consistently less aligned with that of the physics operator C_w .

Quantity of Interest	Sensitive Parameters	NRMSE	Similarity
C_w	$c_1 > c_2$	N/A	N/A
\mathcal{G}_{15}	$c_1 > c_2$	0.267455	100%
SSV ₁₅	$c_3 > c_1$	0.766259	50%
SSV ₁₄	$c_3 > c_1$	0.766271	50%
SSV ₁₃	$c_3 > c_1$	0.801278	50%
SSV ₁₂	$c_3 > c_1$	0.801279	50%
SSV ₁₁	$c_3 > c_1$	0.839496	50%
SSV ₁₀	$c_3 > c_1$	0.839486	50%
SSV ₉	c_3	0.877892	0%
SSV ₈	c_3	0.877874	0%
SSV ₇	c_3	0.908029	0%
SSV ₆	c_3	0.908006	0%
SSV ₅	c_3	0.911654	0%
SSV ₄	c_3	0.911578	0%
SSV ₃	$c_3 > c_2$	0.865169	50%
SSV ₂	$c_3 > c_2$	0.864787	50%

Table 1: Comparison among C_w , SSV, and \mathcal{G} -based sensitivity analyses. The second column displays the order of sensitive parameters concerning the respective quantity of interest. The third and fourth columns present the error (40a) and discrete similarity (40b) between sensitivity indices evaluated with respect to \mathcal{G}_{15} and SSV_{*n*} compared to the indices obtained with C_w .

5.6 Computational cost

The computational cost to perform sensitivity analysis with geometric operators is significantly less than performing these analysis with C_w . On a PC with Intel(R) Xeon(R) Gold 6226 CPU with 2.70 GHz and 2.69 GHz processors and 128 GB of memory on average, each run of the IGA-BEM solver to evaluate C_w took about 540 seconds, totalling around 210 hours to produce Figure 9. In contrast, both the SSV-based analysis and the \mathcal{G} -based analysis required computational time in the order of seconds. To compare the per-run computational cost of C_w versus SSV (10) and \mathcal{G} (32), a benchmark across 50 random samples was performed for all operators to establish, for a given order, the necessary computational cost. These results can be seen in Figure 26, where one can readily notice that for the tested orders, SSV is at least four orders of magnitude faster than C_w , and \mathcal{G} is about 1 to 2 orders of magnitude faster than SSV. It is noteworthy that as the order increases, the computational cost of SSV rises much faster than that of \mathcal{G} , which can be attributed to the number of new moments that each order introduces.

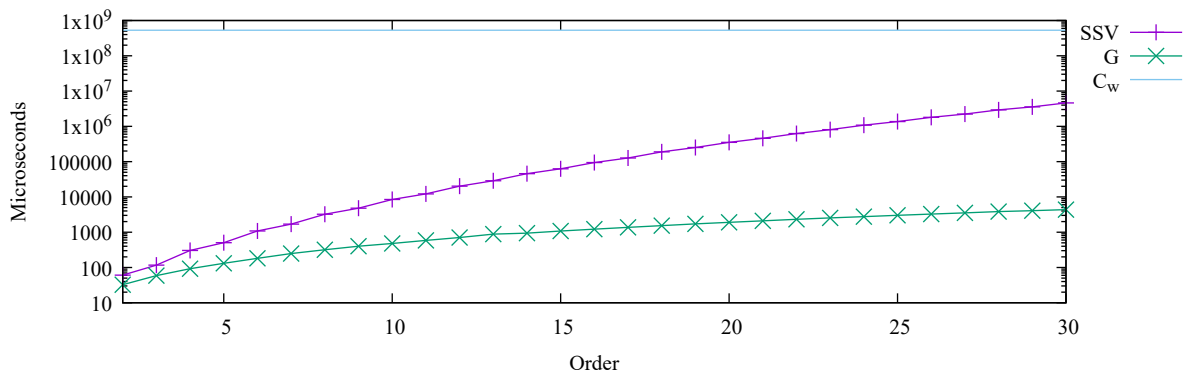


Figure 26: Per-run computational cost of evaluating C_w , SSV and \mathcal{G} verses the order of SSV and \mathcal{G} .

6 Conclusion and Future Work

This study proposes a geometry-based operator to support computationally demanding physical models for reducing the dimensionality of the problem through sensitivity analysis. A general framework for matching physics-based quantities \mathcal{P} to geometry-based ones is outlined in Figure 2. Two geometry-based operators are proposed: the SSV, previously tested in [12], and the slender body operator \mathcal{G} , derived in this paper based on slender body theory. Choosing $\mathcal{P} = C_w$ as the wave resistance coefficient and \mathcal{D} as the modified Wigley hull parametric modeller, the framework is applied twice: once to investigate the compatibility between C_w and SSV, and once for C_w and \mathcal{G} .

The results indicate that \mathcal{G} outperforms SSV significantly, as summarised in Table 1. In this table, one can observe that the slender body operator outperforms SSV for all displayed orders, achieving 100% similarity to C_w while also preserving the relative importance of the sensitive parameters. Furthermore, the computational cost of the

\mathcal{G} -based operator was significantly less than that of C_w , with the former taking seconds and the latter taking days. Additionally, as shown in Figure 26, the computational cost of \mathcal{G} is significantly lower than that of SSV, a difference that becomes more pronounced as the order increases.

While the slender body operator has proven to be a promising candidate geometric operator for the problem of wave resistance when paired with the parametric modeller (41), several avenues have not been explored in this study. First and foremost, the framework of Figure 2 was applied only for one parametric modeller, which also has a small number of parameters. Further experimentation with richer parametric modellers is necessary to expand the applicability of the pair $\mathcal{G} - \mathcal{P}$. The two parametric modellers tested in [12], for which SSV performed satisfactorily, are promising candidates in this regard, allowing for a more in-depth investigation into the seemingly better performance of \mathcal{G} compared to SSV.

Next, the relatively short computational times of the \mathcal{G} -based analysis can be attributed in part to the closed-form expression for the moments (72), made possible by the simple analytical expression of (41). However, it is acknowledged that this may not be possible with more complicated geometries. Nevertheless, relevant experimentation has shown that the increase in computational time is not drastic in the general-surface case, still providing a significant reduction when compared to the C_w -based sensitivity analysis.

Finally, there is potential to enhance \mathcal{G} further by considering the generalised formulation of Vossers' integral, as provided in [45]. This has the potential to increase the performance of the slender body operator.

ACKNOWLEDGEMENTS

This work received funding from the European Union's Horizon 2020 research and innovation programme under the Marie Skłodowska-Curie grant agreement No 860843, PI for the University of Strathclyde: P.D. Kaklis.

References

- [1] L. Sun, H. Gao, S. Pan, J.-X. Wang, Surrogate modeling for fluid flows based on physics-constrained deep learning without simulation data, *Computer Methods in Applied Mechanics and Engineering* 361 (2020) 112732.
- [2] M. Köppen, The curse of dimensionality, in: 5th online world conference on soft computing in industrial applications (WSC5), Vol. 1, 2000, pp. 4–8.
- [3] S. Khan, M. J. Awan, A generative design technique for exploring shape variations, *Advanced Engineering Informatics* 38 (2018) 712–724.
- [4] S. Chen, J. Montgomery, A. Bolufé-Röhler, Measuring the curse of dimensionality and its effects on particle swarm optimization and differential evolution, *Applied Intelligence* 42 (2015) 514–526.
- [5] Z. Masood, S. Khan, L. Qian, Machine learning-based surrogate model for accelerating simulation-driven optimisation of hydropower kaplan turbine, *Renewable Energy* 173 (2021) 827–848.
- [6] D. D'Agostino, A. Serani, E. F. Campana, M. Diez, Nonlinear methods for design-space dimensionality reduction in shape optimization, in: *International Workshop on Machine Learning, Optimization, and Big Data*, Springer, 2017, pp. 121–132.
- [7] P. G. Constantine, E. Dow, Q. Wang, Active subspace methods in theory and practice: Applications to kriging surfaces, *SIAM Journal on Scientific Computing* 36 (4) (2014) A1500–A1524.
- [8] S. Khan, P. Kaklis, From regional sensitivity to intra-sensitivity for parametric analysis of free-form shapes: Application to ship design, *Advanced Engineering Informatics* 49 (2021) 101314.
- [9] A. Saltelli, M. Ratto, T. Andres, F. Campolongo, J. Cariboni, D. Gatelli, M. Saisana, S. Tarantola, *Global Sensitivity Analysis: The Primer*, Wiley, 2008.
- [10] A. Saltelli, P. Annoni, How to avoid a perfunctory sensitivity analysis, *Environmental Modelling & Software* 25 (12) (2010) 1508–1517.
- [11] D. Cacuci, *Sensitivity & Uncertainty Analysis, Volume 1: Theory*, no. v. 1, CRC Press, 2003.
- [12] S. Khan, P. Kaklis, A. Serani, M. Diez, Geometric moment-dependent global sensitivity analysis without simulation data: Application to ship hull form optimisation, *Computer-Aided Design* 151 (2022) 103339.
- [13] K. Cheng, Z. Lu, C. Ling, S. Zhou, Surrogate-assisted global sensitivity analysis: an overview, *Structural and Multidisciplinary Optimization* 61 (2020) 1187–1213.
- [14] B. Iooss, P. Lemaître, *A Review on Global Sensitivity Analysis Methods*, Springer US, Boston, MA, 2015, pp. 101–122.

- [15] H. W. Bode, et al., *Network analysis and feedback amplifier design* (1945).
- [16] E. Borgonovo, E. Plischke, Sensitivity analysis: A review of recent advances, *European Journal of Operational Research* 248 (3) (2016) 869–887.
- [17] I. M. Sobol', On sensitivity estimation for nonlinear mathematical models, *Matematicheskoe modelirovanie* 2 (1) (1990) 112–118.
- [18] F. Gamboa, A. Janon, T. Klein, A. Lagnoux, Sensitivity indices for multivariate outputs, *Comptes Rendus Mathematique* 351 (7) (2013) 307–310.
- [19] F. Sarrazin, F. Pianosi, T. Wagener, Global sensitivity analysis of environmental models: Convergence and validation, *Environmental Modelling & Software* 79 (2016) 135–152.
- [20] C. O. S. Sorzano, J. Vargas, A. P. Montano, A survey of dimensionality reduction techniques, *arXiv preprint arXiv:1403.2877* (2014).
- [21] S. Han, Y.-S. Lee, Y. B. Choi, Hydrodynamic hull form optimization using parametric models, *Journal of marine science and technology* 17 (2012) 1–17.
- [22] D. Zhang, G. Lu, et al., A comparative study of fourier descriptors for shape representation and retrieval, in: *Proc. 5th Asian Conference on Computer Vision*, Citeseer, 2002, p. 35.
- [23] E. Rahtu, M. Salo, J. Heikkilä, A new convexity measure based on a probabilistic interpretation of images, *IEEE Transactions on Pattern Analysis and Machine Intelligence* 28 (9) (2006) 1501–1512.
- [24] P. Corcoran, P. Mooney, A. C. Winstanley, A convexity measure for open and closed contours (2011).
- [25] M. Stojmenović, J. Žunić, Measuring elongation from shape boundary, *Journal of Mathematical Imaging and Vision* 30 (2008) 73–85.
- [26] J. A. Shohat, J. D. Tamarkin, *The problem of moments*, Vol. 1, American Mathematical Society (RI), 1950.
- [27] A. Cuyt, G. Golub, P. Milanfar, B. Verdonk, Multidimensional integral inversion, with applications in shape reconstruction, *SIAM Journal on Scientific Computing* 27 (3) (2005) 1058–1070. [arXiv:https://doi.org/10.1137/030601703](https://doi.org/10.1137/030601703), doi:10.1137/030601703. URL <https://doi.org/10.1137/030601703>
- [28] P. Milanfar, M. Putinar, J. Varah, B. Gustafsson, G. H. Golub, Shape reconstruction from moments: theory, algorithms, and applications, in: *Advanced signal processing algorithms, architectures, and implementations X*, Vol. 4116, SPIE, 2000, pp. 406–416.
- [29] A. Kousholt, J. Schulte, Reconstruction of convex bodies from moments, *Discrete & Computational Geometry* 65 (1) (2021) 1–42.
- [30] F. Ghorbel, S. Derrode, S. Dhahbi, R. Mezhoud, et al., Reconstructing with geometric moments, in: *Proc. int. conf. on machine intelligence: Acidca-icmi*, 2005, pp. 5–7.
- [31] J. M. Pozo, M.-C. Villa-Uriol, A. F. Frangi, Efficient 3d geometric and zernike moments computation from unstructured surface meshes, *IEEE Transactions on Pattern Analysis and Machine Intelligence* 33 (3) (2010) 471–484.
- [32] P. Diaconis, Application of the method of moments in probability and statistics, *Moments in mathematics* 37 (1987) 125–142.
- [33] C.-H. Teh, R. T. Chin, On image analysis by the methods of moments, *IEEE Transactions on pattern analysis and machine intelligence* 10 (4) (1988) 496–513.
- [34] M. I. Sezan, H. Stark, Incorporation of a priori moment information into signal recovery and synthesis problems, *Journal of mathematical analysis and applications* 122 (1) (1987) 172–186.
- [35] S. Khan, P. Kaklis, A. Serani, M. Diez, K. Kostas, Shape-supervised dimension reduction: Extracting geometry and physics associated features with geometric moments, *Computer-Aided Design* 150 (2022) 103327.
- [36] P. Milanfar, G. C. Verghese, W. C. Karl, A. S. Willsky, Reconstructing polygons from moments with connections to array processing, *IEEE Transactions on signal processing* 43 (2) (1995) 432–443.
- [37] P. Milanfar, W. C. Karl, A. S. Willsky, A moment-based variational approach to tomographic reconstruction, *IEEE Transactions on Image Processing* 5 (3) (1996) 459–470.
- [38] V. Strakhov, M. Brodsky, On the uniqueness of the inverse logarithmic potential problem, *SIAM Journal on Applied Mathematics* 46 (2) (1986) 324–344.

- [39] M. Brodsky, E. Panakhov, Concerning a priori estimates of the solution of the inverse logarithmic potential problem, *Inverse problems* 6 (3) (1990) 321.
- [40] S. Khan, K. Goucher-Lambert, K. Kostas, P. Kaklis, Shiphullgan: A generic parametric modeller for ship hull design using deep convolutional generative model, *Computer Methods in Applied Mechanics and Engineering* 411 (2023) 116051.
- [41] G. Vossers, Some applications of the slender body theory in ship hydrodynamics (1962).
- [42] W. Hoeffding, A class of statistics with asymptotically normal distribution, *Breakthroughs in Statistics: Foundations and Basic Theory* (1992) 308–334.
- [43] I. J. Journée, Experiments and calculations on four wigley hullforms, Delft University 909 (1992).
- [44] J. V. Wehausen, The wave resistance of ships, *Advances in applied mechanics* 13 (1973) 93–245.
- [45] H. Maruo, Calculation of the wave resistance of ships, the draught of which is as small as the beam, *Journal of Zosen Kiokai* 1962 (112) (1962) 21–37.
- [46] E. Tuck, On vossers’ integral, in: *International Seminar on Theoretical Wave Resistance*, Ann Arbor, Michigan, 1963, 1963.
- [47] E. Tuck, A systematic asymptotic expansion procedure for slender ships, *Journal of Ship Research* 8 (03) (1964) 15–23.
- [48] J. Kotik, Various wave resistance theories for slender ships, *Schiffstechnik* 10 (54) (1963) 178–186.
- [49] H. Lackenby, On the systematic geometrical variation of ship forms, vol. 92, *Transaction of Royal Institute of Naval Architects* (1950).
- [50] M. Tasrief, M. Kashiwagi, Improvement of Ship Geometry by Optimizing the Sectional Area Curve With Binary-Coded Genetic Algorithms (BCGAs), Vol. All Days of International Ocean and Polar Engineering Conference, 2013.
- [51] K. Belibassakis, T. Gerostathis, K. Kostas, C. Politis, P. Kaklis, A. Ginnis, C. Feurer, A bem-isogeometric method for the ship wave-resistance problem, *Ocean Engineering* 60 (2013) 53–67.

A Convergence of the Slender Body Operator

In this section we show the convergence of (32), for which a comparison and a ratio test suffice. For $S(x)$ the sectional area curve of the hull at the longitudinal position x assume that there exists an $M > 0$ with,

$$|S''(x)| \leq M, \quad \forall x. \quad (48)$$

Then,

$$S''(x)S''(\xi)(x - \xi)^{2k} \leq M^2(x - \xi)^{2k}, \quad \forall x, \xi. \quad (49)$$

Looking at (21) and since the right-hand side of (49) is certainly integrable,

$$\begin{aligned} I_k &= \int_{-L/2}^{L/2} \int_{-L/2}^{L/2} S''(x)S''(\xi)(x - \xi)^{2k} dx d\xi \\ &\leq M^2 \int_{-L/2}^{L/2} \int_{-L/2}^{L/2} (x - \xi)^{2k} dx d\xi \\ &= M^2 \int_{-L/2}^{L/2} \left[\frac{(x - \xi)^{2k+1}}{2k + 1} \right]_{-L/2}^{L/2} d\xi \\ &= \frac{M^2}{2k + 1} \left[\frac{-(L/2 - \xi)^{2k+2} + (-L/2 - \xi)^{2k+2}}{2k + 2} \right]_{-L/2}^{L/2} \\ &= \frac{2M^2 L^{2k+2}}{(2k + 1)(2k + 2)}. \end{aligned} \quad (50)$$

Using (50) and looking at (32),

$$|f(k; K)I_k| \leq |f(k; K)| \frac{2M^2 L^{2k+2}}{(2k + 1)(2k + 2)}, \quad (51)$$

which means that it is enough to show that the following series is absolutely convergent,

$$\sum_{k=0}^{\infty} \beta_k, \quad \beta_k = f(k; K) \frac{2M^2 L^{2k+2}}{(2k+1)(2k+2)}. \quad (52)$$

This can be done by application of the ratio test,

$$\begin{aligned} \frac{|\beta_{k+1}|}{|\beta_k|} &= \frac{f(k+1; K)}{f(k; K)} L^2 \frac{(2k+1)(2k+2)}{(2k+3)(2k+4)} \\ &= \frac{|f(k+1; K)|}{|f(k; K)|} O(1), \quad k \rightarrow \infty. \end{aligned} \quad (53)$$

Then, recalling the definition of $f(k; K)$ from (18),

$$\begin{aligned} \frac{|f(k+1; K)|}{|f(k; K)|} &= \frac{K^2 2^{2k-1} (k!)^2}{2^{2k+1} ((k+1)!)^2} \cdot \frac{\ln(0.5K) + \gamma - h(k+1)}{\ln(0.5K) + \gamma - h(k)} \\ &= \frac{K^2}{4(k+1)^2} \cdot \frac{\ln(0.5K) + \gamma - h(k+1)}{\ln(0.5K) + \gamma - h(k)} \\ &= \frac{\ln(0.5K) + \gamma - h(k+1)}{\ln(0.5K) + \gamma - h(k)} O(k^{-2}), \quad k \rightarrow \infty. \end{aligned} \quad (54)$$

Now, for the harmonic series $h(k)$, it is true that $h(k) = O(\ln(k))$, $k \rightarrow \infty$. In light of this,

$$\begin{aligned} \frac{\ln(0.5K) + \gamma - h(k+1)}{\ln(0.5K) + \gamma - h(k)} &= \frac{h(k+1)}{h(k)} \cdot \frac{1 - \frac{\ln(0.5K) + \gamma}{h(k+1)}}{1 - \frac{\ln(0.5K) + \gamma}{h(k)}} \\ &= \frac{\sum_{i=0}^{k+1} \frac{1}{i}}{\sum_{i=0}^k \frac{1}{i}} \cdot \frac{1 - O((\ln(k+1))^{-1})}{1 - O((\ln(k))^{-1})} \\ &= \left(1 + \frac{1}{(k+1)h(k)}\right) \cdot \frac{1 + o(1)}{1 + o(1)} \\ &= (1 + O(k^{-1}(\ln(k))^{-1}))(1 + o(1)) \\ &= 1 + o(1), \quad k \rightarrow \infty. \end{aligned} \quad (55)$$

Substituting (55) into (54),

$$\frac{|f(k+1; K)|}{|f(k; K)|} = (1 + o(1))O(k^{-2}) = o(1), \quad k \rightarrow \infty. \quad (56)$$

Substituting (56) into (53),

$$\frac{|\beta_{k+1}|}{|\beta_k|} = o(1), \quad k \rightarrow \infty, \quad (57)$$

which means that $\{\beta_i\}$ is an absolutely convergent series. By comparison, (51) implies that

$$\lim_{n \rightarrow \infty} \mathcal{G}(n) \text{ exists and } \in \mathbb{R}. \quad (58)$$

B Closed Forms of the Geometric Moments of the Modified Wigley Hull

In this section, we express the moments (2) and (4) for (41) analytically. We begin with $M(p, q, r)$ by substituting (41) into (2),

$$\begin{aligned} M(p, q, r) &= \int_{-L/2}^{L/2} \int_0^T \int_{-B\eta/2}^{B\eta/2} x^p y^q z^r dy dz dx \\ &= \int_{-L/2}^{L/2} \int_0^T x^p z^r \left[\frac{y^{q+1}}{q+1} \right]_{-B\eta/2}^{B\eta/2} dz dx \\ &= \left(\frac{B}{2}\right)^{q+1} \frac{(1 - (-1)^{q+1})}{q+1} \int_{-L/2}^{L/2} \int_0^T x^p z^r \eta^{q+1} dz dx. \end{aligned} \quad (59)$$

Notice that if q is odd then $M(p, q, r) = 0$ which can be attributed to the breadth-wise symmetry of the Wigley hull. Assuming q to be even, we write

$$M(p, q, r) = \left(\frac{B}{2}\right)^{q+1} \frac{2}{q+1} \int_{-L/2}^{L/2} \int_0^T x^p z^r \eta^{q+1} dz dx, \quad q = \text{even}. \quad (60)$$

To proceed, we expand η^{q+1} ,

$$\begin{aligned} \eta^{q+1} &= \left((1 - \zeta^2)(1 - \xi^2)(1 + c_1 \xi^2 + c_2 \xi^4) + c_3 \zeta^2 (1 - \zeta^8)(1 - \xi^2)^4 \right)^{q+1} \\ &= \sum_{i_1=0}^{q+1} \binom{q+1}{i_1} \left((1 - \zeta^2)(1 - \xi^2)(1 + c_1 \xi^2 + c_2 \xi^4) \right)^{q+1-i_1} \left(c_3 \zeta^2 (1 - \zeta^8)(1 - \xi^2)^4 \right)^{i_1} \\ &= \sum_{i_1=0}^{q+1} \binom{q+1}{i_1} (1 - \zeta^2)^{q+1-i_1} (1 - \xi^2)^{q+1+3i_1} (1 + c_1 \xi^2 + c_2 \xi^4)^{q+1-i_1} c_3^{i_1} \zeta^{2i_1} (1 - \zeta^8)^{i_1} \\ &= \sum_{i_1=0}^{q+1} \binom{q+1}{i_1} \left(\sum_{i_2=0}^{q+1-i_1} \binom{q+1-i_1}{i_2} (-1)^{i_2} \zeta^{2i_2} \right) \left(\sum_{i_3=0}^{q+1+3i_1} \binom{q+1+3i_1}{i_3} (-1)^{i_3} \zeta^{2i_3} \right) \\ &\quad \cdot \left(\sum_{i_4=0}^{q+1-i_1} \binom{q+1-i_1}{i_4} (c_1 \xi^2 + c_2 \xi^4)^{i_4} \right) c_3^{i_1} \zeta^{2i_1} \left(\sum_{i_6=0}^{i_1} \binom{i_1}{i_6} (-1)^{i_6} \zeta^{8i_6} \right) \\ &= \sum_{i_1=0}^{q+1} \binom{q+1}{i_1} \left(\sum_{i_2=0}^{q+1-i_1} \binom{q+1-i_1}{i_2} (-1)^{i_2} \zeta^{2i_2} \right) \left(\sum_{i_3=0}^{q+1+3i_1} \binom{q+1+3i_1}{i_3} (-1)^{i_3} \zeta^{2i_3} \right) \\ &\quad \cdot \left(\sum_{i_4=0}^{q+1-i_1} \binom{q+1-i_1}{i_4} \sum_{i_5=0}^{i_4} \binom{i_4}{i_5} c_1^{i_5} \xi^{2i_5} c_2^{i_4-i_5} \xi^{4i_4-4i_5} \right) c_3^{i_1} \zeta^{2i_1} \left(\sum_{i_6=0}^{i_1} \binom{i_1}{i_6} (-1)^{i_6} \zeta^{8i_6} \right). \end{aligned} \quad (61)$$

Grouping together all the sum-operators and combining common factors,

$$\begin{aligned} \eta^{q+1} &= \sum_{i_1=0}^{q+1} \sum_{i_2=0}^{q+1-i_1} \sum_{i_3=0}^{q+1+3i_1} \sum_{i_4=0}^{q+1-i_1} \sum_{i_5=0}^{i_4} \sum_{i_6=0}^{i_1} \binom{q+1}{i_1} \binom{q+1-i_1}{i_2} \binom{q+1+3i_1}{i_3} \\ &\quad \cdot \binom{q+1-i_1}{i_4} \binom{i_4}{i_5} \binom{i_1}{i_6} (-1)^{i_2+i_3+i_6} c_1^{i_5} c_2^{i_4-i_5} c_3^{i_1} \zeta^{2i_1+2i_2+8i_6} \xi^{2i_3+4i_4-2i_5}. \end{aligned} \quad (62)$$

Substituting (62) into (60) and factoring all constants out of the double integral,

$$\begin{aligned} M(p, q, r) &= \left(\frac{B}{2}\right)^{q+1} \frac{2}{q+1} \sum_{i_1=0}^{q+1} \sum_{i_2=0}^{q+1-i_1} \sum_{i_3=0}^{q+1+3i_1} \sum_{i_4=0}^{q+1-i_1} \sum_{i_5=0}^{i_4} \sum_{i_6=0}^{i_1} \left[\right. \\ &\quad \left. \binom{q+1}{i_1} \binom{q+1-i_1}{i_2} \binom{q+1+3i_1}{i_3} \binom{q+1-i_1}{i_4} \binom{i_4}{i_5} \binom{i_1}{i_6} \right. \\ &\quad \left. \cdot (-1)^{i_2+i_3+i_6} c_1^{i_5} c_2^{i_4-i_5} c_3^{i_1} \int_{-L/2}^{L/2} \xi^{2i_3+4i_4-2i_5} x^p dx \int_0^T \zeta^{2i_1+2i_2+8i_6} z^r dz \right], \quad q = \text{even}. \end{aligned} \quad (63)$$

Since $\xi = 2x/L$,

$$\begin{aligned} \int_{-L/2}^{L/2} \xi^{2i_3+4i_4-2i_5} x^p dx &= (2/L)^{2i_3+4i_4-2i_5} \int_{-L/2}^{L/2} x^{p+2i_3+4i_4-2i_5} dx \\ &= (2/L)^{2i_3+4i_4-2i_5} \left[\frac{x^{p+2i_3+4i_4-2i_5+1}}{p+2i_3+4i_4-2i_5+1} \right]_{-L/2}^{L/2} \\ &= \left(\frac{L}{2}\right)^{p+1} \frac{(1 - (-1)^{p+1})}{p+2i_3+4i_4-2i_5+1}. \end{aligned} \quad (64)$$

Again, if p is odd, $M(p, q, r) = 0$ which can be attributed to the length-wise symmetry of the Wigley hull. Assuming that p is even,

$$\int_{-L/2}^{L/2} \xi^{2i_3+4i_4-2i_5} x^p dx = \left(\frac{L}{2}\right)^{p+1} \frac{2}{p+2i_3+4i_4-2i_5+1}, \quad p = \text{even}. \quad (65)$$

Similarly for $\zeta = z/T$,

$$\int_0^T \zeta^{2i_1+2i_2+8i_6} z^r dz = T^{r+1} \frac{1}{r+2i_1+2i_2+8i_6+1}. \quad (66)$$

Substituting (65) and (66) into (63),

$$M(p, q, r) = \left(\frac{L}{2}\right)^{p+1} \left(\frac{B}{2}\right)^{q+1} T^{r+1} \frac{4}{q+1} \sum_{i_1=0}^{q+1} \sum_{i_2=0}^{q+1-i_1} \sum_{i_3=0}^{q+1+3i_1} \sum_{i_4=0}^{q+1-i_1} \sum_{i_5=0}^{i_4} \sum_{i_6=0}^{i_1} \left[\begin{aligned} & \binom{q+1}{i_1} \binom{q+1-i_1}{i_2} \binom{q+1+3i_1}{i_3} \binom{q+1-i_1}{i_4} \binom{i_4}{i_5} \binom{i_1}{i_6} \\ & \cdot (-1)^{i_2+i_3+i_6} c_1^{i_5} c_2^{i_4-i_5} c_3^{i_1} (p+2i_3+4i_4-2i_5+1)^{-1} (r+2i_1+2i_2+8i_6+1)^{-1} \end{aligned} \right], \quad (67)$$

where $p, q = \text{even}$.

The presentation of (67) can be simplified considerably by noticing that the sums can be split into three groups: the first group consists only of the sum with index i_1 , the second group of the sums with indexes $\{i_3, i_4, i_5\}$ and the final group with $\{i_2, i_6\}$. Then,

$$M(p, q, r) = \begin{cases} \left(\frac{L}{2}\right)^{p+1} \left(\frac{B}{2}\right)^{q+1} T^{r+1} \frac{4}{q+1} \sum_{i_1=0}^{q+1} \binom{q+1}{i_1} c_3^{i_1} \mathcal{X}_{i_1} \mathcal{Z}_{i_1}, & p, q \text{ are even} \\ 0, & \text{else,} \end{cases} \quad (68a)$$

where

$$\mathcal{X}_{i_1} = \sum_{i_3=0}^{q+1+3i_1} \sum_{i_4=0}^{q+1-i_1} \sum_{i_5=0}^{i_4} \binom{q+1+3i_1}{i_3} \binom{q+1-i_1}{i_4} \binom{i_4}{i_5} (-1)^{i_3} c_1^{i_5} c_2^{i_4-i_5} (p+2i_3+4i_4-2i_5+1)^{-1}, \quad (68b)$$

and

$$\mathcal{Z}_{i_1} = \sum_{i_2=0}^{q+1-i_1} \sum_{i_6=0}^{i_1} \binom{q+1-i_1}{i_2} \binom{i_1}{i_6} (-1)^{i_2+i_6} (r+2i_1+2i_2+8i_6+1)^{-1}. \quad (68c)$$

Having (68a) it is easy to evaluate an analogous expression for the translation invariant moment $M_T(p, q, r)$. as given in (4),

$$M_T(p, q, r) = \int_{-L/2}^{L/2} \int_0^T \int_{-B\eta/2}^{B\eta/2} (x - C_x)^p (y - C_y)^q (z - C_z)^r dy dz dx. \quad (69)$$

First, notice that by (68a), $M(1, 0, 0) = M(0, 1, 0) = 0$. Then, looking at (3), $C_x = C_y = 0$,

$$M_T(p, q, r) = \int_{-L/2}^{L/2} \int_0^T \int_{-B\eta/2}^{B\eta/2} x^p y^q (z - C_z)^r dy dz dx. \quad (70)$$

In the derivation of (68a), the z^r factor (now $(z - C_z)^r$) was integrated at (66). One can then easily be convinced that the only difference between $M_T(p, q, r)$ and (68a) will be in \mathcal{Z}_{i_1} . Specifically, looking at (66)

$$\begin{aligned} \int_0^T \zeta^{2i_1+2i_2+8i_6} (z - C_z)^r dz &= \left(T^{2i_1+2i_2+8i_6}\right)^{-1} \int_0^T z^{2i_1+2i_2+8i_6} \sum_{j=0}^r \binom{r}{j} z^{r-j} (-1)^j C_z^j dz \\ &= \left(T^{2i_1+2i_2+8i_6}\right)^{-1} \sum_{j=0}^r \binom{r}{j} (-1)^j C_z^j \left[\frac{z^{r+2i_1+2i_2+8i_6-j+1}}{r+2i_1+2i_2+8i_6-j+1} \right]_0^T \\ &= T^{r+1} \sum_{j=0}^r \binom{r}{j} (-1)^j \left(\frac{C_z}{T}\right)^j (r+2i_1+2i_2+8i_6-j+1)^{-1}. \end{aligned} \quad (71)$$

So that finally,

$$M_T(p, q, r) = \begin{cases} \left(\frac{L}{2}\right)^{p+1} \left(\frac{B}{2}\right)^{q+1} T^{r+1} \frac{4}{q+1} \sum_{i_1=0}^{q+1} \binom{q+1}{i_1} c_3^{i_1} \mathcal{X}_{i_1} \mathcal{Z}_{i_1}, & p, q \text{ are even} \\ 0, & \text{else,} \end{cases} \quad (72a)$$

with

$$\mathcal{Z}_{i_1} = \sum_{i_2=0}^{q+1-i_1} \sum_{i_6=0}^{i_1} \sum_{j=0}^r \binom{q+1-i_1}{i_2} \binom{i_1}{i_6} \binom{r}{j} (-1)^{i_2+i_6+j} \left(\frac{C_z}{T}\right)^j (r+2i_1+2i_2+8i_6-j+1)^{-1}, \quad (72b)$$

where C_z is given by (3) and \mathcal{X}_{i_1} by (68b). It should be noted that the validity of equations (68) and (72) were verified via the computer algebraic system in MAPLE[©] 4.

C Closed Form of the Sectional Area Curve of the Modified Wigley Hull

In this section, a closed form for the sectional area of (41) at a given longitudinal position $x \in [-L/2, L/2]$, $S(x)$, is derived. We can directly write

$$S(x) = \int_0^T \int_{-B\eta/2}^{B\eta/2} dy dz = B \int_0^T \eta dz = B(1-\xi^2)(1+c_1\xi^2+c_2\xi^4) \int_0^T (1-\zeta^2) dz + Bc_3(1-\xi^2)^4 \int_0^T (\zeta^2-\zeta^{10}) dz \quad (73)$$

where $\xi = 2x/L$ and $\zeta = z/T$. Evaluating the integrals in (73),

$$S(x) = BT \left(\frac{2}{3}(1-\xi^2)(1+c_1\xi^2+c_2\xi^4) + \frac{8c_3}{33}(1-\xi^2)^4 \right) \quad (74)$$

Differentiating (74) with respect to x ,

$$S'(x) = \frac{2BT}{L} \left(-\frac{4\xi}{3}(1+c_1\xi^2+c_2\xi^4) + \frac{2}{3}(1-\xi^2)(2c_1\xi+4c_2\xi^3-32c_3\xi(1-\xi^2)^2/11) \right) \quad (75)$$

For $x = \pm L/2$, $\xi(x = \pm L/2) = \pm 1$ we get,

$$S'(\pm L/2) = \mp \frac{8BT}{3L} (1+c_1+c_2) \quad (76)$$

which attains its maximum at $c_1 = c_2 = 1$, $|S'(\pm L/2; c_1 = c_2 = 1)| = 8BT/L$

⁴<https://www.maplesoft.com/products/Maple/>